# Online damage detection in structural systems via dynamic inverse analysis: a recursive Bayesian approach

*S. Eftekhar Azam*[1*], *S. Mariani*[2]

[1] Department of Civil Engineering, University of Nebraska–Lincoln, Lincoln, USA
[2] Department of Civil and Environmental Engineering, Politecnico di Milano, Milano, ITALY

## ABSTRACT

In this paper, a framework is presented for the joint state tracking and parameter estimation of partially observed structural systems characterized by a relatively large number of degrees of freedom. To pursue this aim in real-time, the order of the system is reduced via an optimal set of bases, or proper orthogonal modes (POMs) obtained through proper orthogonal decomposition. Since the aforementioned POMs are sensitive to damage, which is defined as a change in the stiffness of the structural model, the variation in the characteristics of the POMs themselves is also tracked online. Taking advantage of the linear relationship between the observation process and the components of the POMs, a solution to the whole problem is obtained with an extended Kalman filter or a hybrid extended Kalman particle filter for the joint tracking-estimation purposes, and with a further Kalman filter for the model update purposes. The efficiency of the proposed method is assessed through simulated experiments on a 8-story shear type building.

**Keywords**: structural health monitoring; Kalman filter; hybrid particle filter; proper orthogonal decomposition; model update

* University of Nebraska–Lincoln, Department of Civil Engineering, 2200 Vine St, Lincoln, NE 68503, USA; tel: +1-402 472 1994
Email: eftekhar-azam@unl.edu

## 1. INTRODUCTION

Aging of infrastructures in developed countries, performance based design, and environmental changes all call for systems to monitor in real-time the health of structural systems. The current practice to assess the health and integrity of a structure is predominantly based on visual inspections, whose frequency can vary from once a month to once every a few years, depending on factors related to the age and the importance of the structure itself. Such inspections primarily furnish a qualitative awareness on possible structural defects, and once damage is detected a quantitative evaluation of the remaining lifetime of the structure becomes necessary. The reliability of the said visual inspection is thus primarily related to the capability of the inspector. Recent advances in measurement technology, computing power, and signal processing have provided an unprecedented prospect for developing autonomous, robust and continuous structural health monitoring (SHM) systems. Numerous structures across the globe have been already instrumented by sensors that include strain gages, accelerometers and displacement transducers to quantify their responses. State-of-the-art monitoring schemes in the literature are centered on extracting parameters of a model of the structure from the measured signals, so as to be able to update it and detect, localize, and quantify damage from changes in the system characteristics.

In a physics-based SHM framework, the detection of changes in the mechanical properties of structural members is the main objective. A damage in the structure is considered as a degradation of its stiffness and/or load bearing capacity, see [1]; such degradation may be due to a change of the geometry of the members, or to a reduction of their mechanical properties. Accordingly, the detection of damage in a structure can be posed as a system identification problem. Dealing with a linear structure, i.e. assuming that damage can be temporarily frozen within the time window between two subsequent observation instants, several algorithms can provide an offline identification of the system properties. In the time domain, the data driven stochastic subspace identification algorithm is de facto standard for output only identification of structural models, see [2]; the subspace identification algorithm has been widely applied for deterministic input-output systems, see [3]. The aforementioned methods rest on singular value decomposition (SVD) and QR decomposition techniques, see [4]. They have been also adopted for online system identification by operating on a fixed-length window that moves over time: when a new observation becomes available, the subspace is re-identified. The computational costs associated with SVD and QR techniques prevent the real-time application of such methods for large structural systems; to reduce such costs, methods have been proposed to only update the SVD and QR outcomes, see e.g. [3]. It has been also shown that the measurement noise can substantially affect the performance of these methods, especially when the duration of the moving time-window is assumed short.

To alleviate the issues attributed to modelling and measurement uncertainties in online system identification, recursive Bayesian estimation methods are usually exploited. The online and real-time estimation of the state of a system and of the relevant unknown model parameters is usually obtained by augmenting the state, namely by joining the state to be tracked and the parameters to be tuned into a vector of unknowns, whose dynamics needs to be appropriately modelled. The mentioned unknown model parameters can be the mechanical properties of the system, that for instance vary in time due to variations in the ambient temperature, see [5]. In the literature of online Bayesian estimation, a considerable effort has been devoted to this joint

state-parameter estimation problem, whose results are affected by the type of system evolution. For instance, an extended Kalman filter (EKF) has been adopted in [6] for the identification of constitutive parameters of composite materials, to detect possible delamination/damage events. The unscented Kalman filter has been applied in [7] for the parameter identification of a hysteretic model, see also [8]; a parallel implementation scheme for the same unscented Kalman filter has been proposed in [9], still to deal with impact-induced vibrations and delamination of composite materials. A hybrid extended Kalman particle filter (EK-PF) for the identification of nonlinear structural systems has been offered in [10], in order to better catch the evolution of the statistics of the state variables in the mentioned nonlinear frame. A particle filter with mutation schemes has been applied in [11] for the estimation of time-invariant parameters of structural models. Recursive Bayesian filters have been recently considered also for the online and real-time estimation of fatigue damage [12]. For a review of the literature on this topic, readers are referred to [13, 14].

In this work, to detect damage in real-time a joint estimation of state and stiffness parameters is proposed, by making use of recursive Bayesian filters. As the number of degrees of freedom (DOFs) of the structural model increases, a bias has been already shown to rapidly pollute the estimates furnished by these filters, see [13]. To cope also with this problem, we provide a scheme for the reduced-order modeling of the system; the joint estimation of state and parameters is then carried out on the obtained reduced-order model (ROM) of the structure, and not on the original full-order one [15]. Unlike the identification of the full-order model, estimating stiffness components related to the ROM does not allow to obtain explicit information concerning the intensity and location of the damage state. However, it is known that the proper orthogonal modes (POMs) of a structure, as provided by the model order reduction technique, contain data concerning the location and intensity of a possible damage, see e.g. [16-20]. This feature of POMs can potentially compensate for the aforementioned shortcoming of the joint estimation at the ROM level, and is here specifically exploited. To this end, we therefore discuss an algorithm for the joint estimation of state and parameters of the ROM, accompanied by an online update of the damage-sensitive POMs of the structure. At each recursion of the (discrete time) Bayesian procedure, a Kalman filter is adopted to update the subspace spanned by POMs retained in the ROM; an EKF, or a hybrid EK-PF is instead used to estimate the joint state vector of the ROM. While the EKF-based approach was already discussed in [20], the EF-PF-based approach is newly proposed in this work. The two approaches are comparatively assessed to ascertain whether the superior performance of the EK-PF in tracking the nonlinear evolution of system statistics can actually deliver a SHM system more sensitive to the state of damage. The offered framework is shown to be able to effectively detect the severity of damage in shear type buildings; the efficiency of the methodology is testified through pseudo-experimental data relevant to a multi-story frame, obtained from direct numerical analyses polluted with ad-hoc measurement noise terms.

The remainder of the paper is organized as follows. In Section 2, the state-space formulation of structural dynamics is reviewed, followed by highlights on the key features of the proper orthogonal decomposition (POD)-based model order reduction technique. In Section 3, peculiarities of the joint estimation of the ROM of a damaging structure are discussed; next, the proposed methodology is presented and the intricated formulation to allow for model update is discussed. In Section 4 the efficiency of the approach is numerically assessed by tracking the damage state in a shear type building; some results are also reported for the full-order structural model, to discuss the detrimental effects of a large number of unknown model parameters on

the accuracy of the estimates, and to also compare the performance of the proposed methodology with those based on the EKF or a standard PF. Some concluding remarks on the work done, and suggestions for future developments are then gathered in Section 5. Since the available EKF-based approach is here adotped as a term of comparison, in Appendix A the scheme relevant to this further approach is briefly discussed for completeness, and to provide a uniform notation for the two formulations.

## 2. STRUCTURAL DYNAMICS: STATE-SPACE FORMULATION AND REDUCED-ORDER MODELING

Let us consider a space-discretized structural system, whose dynamics is governed by the vectorial equation:

$$\boldsymbol{M}\ddot{\boldsymbol{u}} + \boldsymbol{D}(t)\dot{\boldsymbol{u}} + \boldsymbol{K}(t)\boldsymbol{u} = \boldsymbol{F}(t) \tag{1}$$

where: $\boldsymbol{u}$, $\dot{\boldsymbol{u}}$ and $\ddot{\boldsymbol{u}}$ are the vectors gathering relevant (nodal, in case of e.g. finite element discretizations) displacements, velocities and accelerations; $\boldsymbol{M}$ is the mass matrix; $\boldsymbol{D}$ is the damping matrix; $\boldsymbol{K}$ is the stiffness matrix; $\boldsymbol{F}$ is the external load vector. If the system is supposed to be continuously monitored to sense possible drifts in its response to the external actions due to the inception or growth of a damage process, the mass matrix can be assumed to be time-invariant. On the other hand, since geometrical and/or stiffness characteristics of some structural members can be affected by the aforementioned damage, $\boldsymbol{K}$ varies in time. In the case of a Rayleigh damping as considered in Section 4, for which the damping properties of the structure are proportional to the stiffness and mass ones, coefficients in $\boldsymbol{D}$ turn out to be damage- and also time-dependent too, see also [21].

With a focus on two-dimensional models of shear type buildings, the mass matrix is a diagonal one with non-zero entries corresponding to the story masses, whilst the stiffness matrix has a characteristic tri-diagonal banded structure, ruled by the properties of the interstory columns. The damping matrix might have a more complex structure, depending on the mechanisms inducing dissipation, see e.g. [22]. The external load vector in this case gathers the horizontal loads acting at each single story level.

To move to a state-space formulation, a time discretization and a stepping scheme are needed for the solution of Eq. (1). Through a Newmark explicit time integration procedure, within a generic time interval $[t_{k-1}\ \ t_k]$ the solution can be updated in accordance with:

- prediction stage:

$$\tilde{\boldsymbol{u}}_k = \boldsymbol{u}_{k-1} + \Delta t\, \dot{\boldsymbol{u}}_{k-1} + \Delta t^2(\tfrac{1}{2} - \beta)\ddot{\boldsymbol{u}}_{k-1} \tag{2}$$

$$\tilde{\dot{\boldsymbol{u}}}_k = \dot{\boldsymbol{u}}_{k-1} + \Delta t(1-\gamma)\ddot{\boldsymbol{u}}_{k-1} \tag{3}$$

- explicit integration stage:

$$\ddot{\boldsymbol{u}}_k = \boldsymbol{M}^{-1}(\boldsymbol{F}_k - (\boldsymbol{D}_{k-1}\,\tilde{\dot{\boldsymbol{u}}}_k + \boldsymbol{K}_{k-1}\,\tilde{\boldsymbol{u}}_k)) \tag{4}$$

- correction stage:

$$\boldsymbol{u}_k = \tilde{\boldsymbol{u}}_k + \Delta t^2 \beta \ddot{\boldsymbol{u}}_k \tag{5}$$

$$\dot{\boldsymbol{u}}_k = \dot{\tilde{\boldsymbol{u}}}_k + \Delta t\, \gamma \ddot{\boldsymbol{u}}_k \tag{6}$$

where: $\Delta t = t_k - t_{k-1}$ denotes the time step size; $\boldsymbol{u}_{k-1}$, $\dot{\boldsymbol{u}}_{k-1}$ and $\ddot{\boldsymbol{u}}_{k-1}$ provide the solution at the beginning of the time step; $\boldsymbol{u}_k$, $\dot{\boldsymbol{u}}_k$ and $\ddot{\boldsymbol{u}}_k$ is the solution to be computed at the end of the same time step; when stiffness and damping are time-varying properties of the system, $\boldsymbol{K}_{k-1}$ and $\boldsymbol{D}_{k-1}$ denote their values at time $t_{k-1}$, so at the beginning of the time step in compliance with the adopted explicit approach, wherein everything is assumed to be known except the parameters defining the kinematics of the structure at $t_k$; $\beta$ and $\gamma$ are algorithmic parameters defining the method, see [23]. To avoid numerical instabilities, for linear systems $\Delta t$ must not exceed a critical threshold $\Delta t_{cr}$ depending on the shortest vibration period of the structure.

By introducing an extended state vector $\boldsymbol{z}_k$ to collect $\boldsymbol{u}_k$, $\dot{\boldsymbol{u}}_k$ and $\ddot{\boldsymbol{u}}_k$ at the same time instant $t_k$, we get:

$$\boldsymbol{z}_k = \begin{bmatrix} \boldsymbol{u}_k \\ \dot{\boldsymbol{u}}_k \\ \ddot{\boldsymbol{u}}_k \end{bmatrix} \tag{7}$$

It was already detailed in [8, 13] that $\boldsymbol{z}_k$ has to collect all the parameters describing the kinematics of the system, otherwise in the nonlinear regime some information would be missed in terms of the statistics of the state evolving according to Eqs. (2)-(6). The relevant fully discretized state-space form of Eq. (1) is thus obtained as:

$$\boldsymbol{z}_k = \boldsymbol{A}_k\, \boldsymbol{z}_{k-1} + \boldsymbol{b}_k \tag{8}$$

where:

$$\boldsymbol{A}_k = \begin{bmatrix} \boldsymbol{I} - \beta\, \Delta t^2 \boldsymbol{M}^{-1}\boldsymbol{K}_{k-1} & \Delta t\, \boldsymbol{I} - \beta\, \Delta t^2 \boldsymbol{M}^{-1}(\boldsymbol{D}_{k-1} + \Delta t\, \boldsymbol{K}_{k-1}) & -\beta\, \Delta t^2 \boldsymbol{M}^{-1}\left(\Delta t^2 \left({}^1/_2 - \beta\right)\boldsymbol{K}_{k-1} + \Delta t(1-\gamma)\, \boldsymbol{D}_{k-1}\right) + \Delta t^2 \left({}^1/_2 - \beta\right) \boldsymbol{I} \\ -\gamma\, \Delta t\, \boldsymbol{M}^{-1}\boldsymbol{K}_{k-1} & \boldsymbol{I} - \gamma\, \Delta t \boldsymbol{M}^{-1}(\boldsymbol{D}_{k-1} + \Delta t\, \boldsymbol{K}_{k-1}) & -\gamma\, \Delta t \boldsymbol{M}^{-1}\left(\Delta t^2 \left({}^1/_2 - \beta\right)\boldsymbol{K}_{k-1} + \Delta t(1-\gamma)\, \boldsymbol{D}_{k-1}\right) + \Delta t(1-\gamma)\, \boldsymbol{I} \\ -\boldsymbol{M}^{-1}\, \boldsymbol{K}_{k-1} & -\boldsymbol{M}^{-1}(\boldsymbol{D}_{k-1} + \Delta t\, \boldsymbol{K}_{k-1}) & -\boldsymbol{M}^{-1}\left(\Delta t^2 \left({}^1/_2 - \beta\right)\boldsymbol{K}_{k-1} + \Delta t(1-\gamma)\, \boldsymbol{D}_{k-1}\right) \end{bmatrix} \tag{9}$$

$$\boldsymbol{b}_k = \begin{bmatrix} \beta\, \Delta t^2 \boldsymbol{M}^{-1}\, \boldsymbol{F}_k \\ \gamma\, \Delta t\, \boldsymbol{M}^{-1} \boldsymbol{F}_k \\ \boldsymbol{M}^{-1} \boldsymbol{F}_k \end{bmatrix} \tag{10}$$

If we further assume that the structural system is at least partially observable, the corresponding observation equation at time $t_k$ reads:

$$\boldsymbol{y}_k = \boldsymbol{H}\boldsymbol{z}_k \tag{11}$$

where: $\boldsymbol{y}_k$ is the vector of observations; $\boldsymbol{H}$ is a Boolean matrix of appropriate dimensions, that links the whole state $\boldsymbol{z}_k$ of the system to the observations $\boldsymbol{y}_k$ with no time delay. As $\boldsymbol{H}$ is time-invariant, it is implicitly assumed that measurements are always collected at the same locations and with the same kind of instrumentation.

In [13], the use of Eqs. (8) and (11) for identification purposes was extensively discussed, especially in terms of the expected accuracy of model calibration and updating (if necessary). It was shown that, by increasing the number of unknown parameters in the structural model, the tracking of the time-varying parameters gets more and more affected by biases. In an effort to reduce the number of model DOFs and, accordingly, of the mentioned state parameters to be tracked in time, in [15] component mode synthesis was adopted: the re-analyses required by

inverse analysis were so efficiently performed in a reduced-order space of generalized coordinates, using exact component modes and characteristic interface modes computed only once for a reference model. In the present study, since the focus is on reducing also the number of damage-driven characteristic model parameters, POD is adopted as already proven successful for surrogate system modelling. Witih similar approaches, in [24] radial basis functions were adopted to interpolate the relevant POMs retained in the ROM for varying parameter values; in [25], POD was used to enable fast and reliable evaluations of aerodynamic fields. In [26], the errors induced by such POD-based surrogate modelling approach were investigated too.

To cope with the mentioned issue of identification accuracy spoiled by an increasing number of state vector components, a ROM of the structural system thus proves useful. As detailed also in [20, 27], in our study we assume that damage and, in turn, stiffness terms in $\boldsymbol{K}(t)$ and damping terms in $\boldsymbol{D}(t)$, evolve smoothly and slowly in time, with a characteristic time-scale much larger than the $\Delta t$ value adopted in the analysis. Accordingly, standard model order reduction methods for linear systems can be adopted also in the present non-linear case with limited errors, provided that some additional model updating strategies are allowed for to continuously track the evolution of damage and also the projection of the full-order model dynamics onto the reduced-order subspace [28].

The state vector $\boldsymbol{z}_k$ is made of displacement, velocity and acceleration components, so a multiplicative decomposition of the solution into space and time variations is handled. The displacement field $\boldsymbol{u} \in \mathbb{R}^m$, where $m$ is the number of DOFs of the system, can accordingly be decomposed as:

$$\boldsymbol{u}(\boldsymbol{x}, t) = \sum_{i=1}^{m} \boldsymbol{\varphi}_i(x)\alpha_i(t) \tag{12}$$

where the orthonormal vectors or modes $\boldsymbol{\varphi}_i(x)$, $i = 1, \dots, m$, catch the mentioned space variation of the solution, whereas the scalar variables $\alpha_i(t)$ provide the corresponding time variation. In many applications, it has been shown that major variations in the structural response to loading occur in a rather small subspace of $\boldsymbol{\Phi} = [\boldsymbol{\varphi}_1 \ \dots \ \boldsymbol{\varphi}_m]$; the evolution of the system can be therefore estimated by employing the first $l$ modes only, with possibly $l \ll m$, via:

$$\boldsymbol{u}(\boldsymbol{x}, t) \approx \sum_{i=1}^{l} \boldsymbol{\varphi}_i(x)\alpha_i(t) = \boldsymbol{\Phi}_l \, \boldsymbol{\alpha} \tag{13}$$

where $\boldsymbol{\Phi}_l$ is the matrix collecting the $l$ modes to be retained in the ROM. Due to the approximation (13), the equation of motion (1) cannot be satisfied exactly. By projecting the relevant residual onto the same space spanned by the modes in matrix $\boldsymbol{\Phi}_l$, we then obtain the reduced-order equation of motion as:

$$\boldsymbol{\mathcal{M}}_l \ddot{\boldsymbol{\alpha}} + \boldsymbol{\mathcal{D}}_l(t)\dot{\boldsymbol{\alpha}} + \boldsymbol{\mathcal{K}}_l(t)\boldsymbol{\alpha} = \boldsymbol{\mathcal{F}}_l(t) \tag{14}$$

where, in compliance with the space-time multiplicative decomposition of the solution:

$$\begin{aligned} \boldsymbol{\mathcal{M}}_l &= {\boldsymbol{\Phi}_l}^{\mathrm{T}} \boldsymbol{M} \boldsymbol{\Phi}_l \\ \boldsymbol{\mathcal{D}}_l &= {\boldsymbol{\Phi}_l}^{\mathrm{T}} \boldsymbol{D} \boldsymbol{\Phi}_l \\ \boldsymbol{\mathcal{K}}_l &= {\boldsymbol{\Phi}_l}^{\mathrm{T}} \boldsymbol{K} \boldsymbol{\Phi}_l \\ \boldsymbol{\mathcal{F}}_l &= {\boldsymbol{\Phi}_l}^{\mathrm{T}} \boldsymbol{F} \end{aligned} \tag{15}$$

are the reduced-order mass, damping and stiffness matrices, and external load vector, respectively; readers are referred to [28] for further details on the considered Galerkin projection.

As anticipated, within the present frame matrix $\boldsymbol{\Phi}_l$ can be computed with any strategy applicable to linear systems. By employing POD, and specifically the snapshot version of POD [29], the structural ROM is built in an initial training stage of the analysis. Within this offline stage, the solution, in terms of displacements, is collected for a certain number $n$ of time instants; such sequence of snapshots of the response is then assembled in the matrix $\boldsymbol{U} = [\boldsymbol{u}_1\ \boldsymbol{u}_2\ \ldots\ \boldsymbol{u}_n]$. Care must be devoted to the sampling procedure during training and to the duration of the training itself, or in other terms to the time spacing between subsequent snapshots (not necessarily exactly equal to $\Delta t$) and to the number $n$: it is in fact important that each snapshot brings new information about system dynamics, featuring minimal correlation with the other snapshots otherwise information becomes unnecessarily redundant. In [30], it was suggested to parametrize the duration of training through the fundamental vibration period of the structure, also checking the convergence of the retained POMs towards a steady state-like solution; in [31, 32], an automatic procedure was instead adopted to update the POMs whenever new information is brought by partially uncorrelated snapshots, then attaining a reduced computational burden.

The current snapshot matrix $\boldsymbol{U}$ can be decomposed according to, see [33]:

$$\boldsymbol{U} = \boldsymbol{L}\boldsymbol{\Sigma}\boldsymbol{R}^{\mathrm{T}} \tag{16}$$

where: $\boldsymbol{L}$ is an orthonormal matrix, whose columns are the left singular vectors of $\boldsymbol{U}$; $\boldsymbol{\Sigma}$ is a pseudo-diagonal and semi-positive definite matrix, whose pivotal entries $\Sigma_{ii}$ are the singular values of $\boldsymbol{U}$; $\boldsymbol{R}$ is an orthonormal matrix, whose columns are the right singular vectors of $\boldsymbol{U}$.

The whole basis set $\boldsymbol{\Phi}$, i.e. the POMs, is given by $\boldsymbol{L}$, see [34]. If the singular values $\Sigma_{ii}$ are sorted in a decreasing order and the columns of $\boldsymbol{L}$ and $\boldsymbol{R}$ are accordingly arranged, the decomposition (16) provides through the first $l$ columns of $\boldsymbol{L}$ the optimal basis subset. Additional reasoning concerning the relationship between singular values and oriented energies, see again [34], allows setting the number $l$ of POMs to be retained in $\boldsymbol{\Phi}_l$ on the basis of the required accuracy of the ROM, measured by the energy fluxes taking place inside the original system. The required accuracy index $p \leq 1$ of the reduced-order solution, intended as a fraction of the total oriented energy of the full-order model, is assigned and the order $l$ of the ROM is provided by fulfilling:

$$\frac{\sum_{i=1}^{l} {\Sigma_{ii}}^2}{\sum_{i=1}^{m} {\Sigma_{ii}}^2} \geq p \tag{17}$$

so through the ratio between the sum of the singular values (squared) of the modes in the ROM and the sum of all the singular values (again squared). Additional details on the procedure within the present context can be found in [13].

In the current reduced-order representation of system evolution, the state vector is built by mimicking Eq. (7) and it thus reads:

$$\boldsymbol{z}_{r,k} = \begin{bmatrix} \boldsymbol{\alpha}_k \\ \dot{\boldsymbol{\alpha}}_k \\ \ddot{\boldsymbol{\alpha}}_k \end{bmatrix} \tag{18}$$

The corresponding state-space time evolution and observation equations are given by:

$$\boldsymbol{z}_{r,k} = \boldsymbol{A}_{l,k}\boldsymbol{z}_{r,k-1} + \boldsymbol{b}_{l,k} \tag{19}$$

$$\boldsymbol{y}_k = \boldsymbol{H}\boldsymbol{C}\,\boldsymbol{z}_{r,k} \tag{20}$$

where:

$$\boldsymbol{A}_{l,k} = \begin{bmatrix} \boldsymbol{I} - \beta\,\Delta t^2 \boldsymbol{\mathcal{M}}_l{}^{-1}\boldsymbol{\mathcal{K}}_{l,k-1} & \Delta t\,\boldsymbol{I} - \beta\,\Delta t^2 \boldsymbol{\mathcal{M}}_l{}^{-1}(\boldsymbol{\mathcal{D}}_{l,k-1} + \Delta t\,\boldsymbol{\mathcal{K}}_{l,k-1}) & -\beta\,\Delta t^2 \boldsymbol{\mathcal{M}}_l{}^{-1}(\Delta t^2(1/2 - \beta)\boldsymbol{\mathcal{K}}_{l,k-1} + \Delta t(1-\gamma)\,\boldsymbol{\mathcal{D}}_{l,k-1}) + \Delta t^2(1/2 - \beta)\,\boldsymbol{I} \\ -\gamma\,\Delta t\,\boldsymbol{\mathcal{M}}_l{}^{-1}\boldsymbol{\mathcal{K}}_{l,k-1} & \boldsymbol{I} - \gamma\,\Delta t \boldsymbol{\mathcal{M}}_l{}^{-1}(\boldsymbol{\mathcal{D}}_{l,k-1} + \Delta t\,\boldsymbol{\mathcal{K}}_{l,k-1}) & -\gamma\,\Delta t \boldsymbol{\mathcal{M}}_l{}^{-1}(\Delta t^2(1/2 - \beta)\boldsymbol{\mathcal{K}}_{l,k-1} + \Delta t(1-\gamma)\,\boldsymbol{\mathcal{D}}_{l,k-1}) + \Delta t(1-\gamma)\,\boldsymbol{I} \\ -\boldsymbol{\mathcal{M}}_l{}^{-1}\boldsymbol{\mathcal{K}}_{l,k-1} & -\boldsymbol{\mathcal{M}}_l{}^{-1}(\boldsymbol{\mathcal{D}}_{l,k-1} + \Delta t\,\boldsymbol{\mathcal{K}}_{l,k-1}) & -\boldsymbol{\mathcal{M}}_l{}^{-1}(\Delta t^2(1/2 - \beta)\boldsymbol{\mathcal{K}}_{l,k-1} + \Delta t(1-\gamma)\,\boldsymbol{\mathcal{D}}_{l,k-1}) \end{bmatrix} \tag{21}$$

$$\boldsymbol{b}_{l,k} = \begin{bmatrix} \beta\,\Delta t^2 \boldsymbol{\mathcal{M}}_l{}^{-1}\,\boldsymbol{\mathcal{F}}_{l,k} \\ \gamma\,\Delta t\,\boldsymbol{\mathcal{M}}_l{}^{-1}\boldsymbol{\mathcal{F}}_{l,k} \\ \boldsymbol{\mathcal{M}}_l{}^{-1}\boldsymbol{\mathcal{F}}_{l,k} \end{bmatrix} \tag{22}$$

In the above equations, the subscript $r$ is used to denote the vectors related to the ROM, whereas the subscript $l$ is used for the structural properties to explicitly highlight that they do depend also on the order of the ROM and not only on the structure itself. It must be then emphasized that different loads in the training stage may lead to different subspaces identified through POD and so to different ROMs, even if all related to the same original full-order model. In Eq. (20), matrix $\boldsymbol{C}$ reads:

$$\boldsymbol{C} = \begin{bmatrix} \boldsymbol{\Phi}_l & & \\ & \boldsymbol{\Phi}_l & \\ & & \boldsymbol{\Phi}_l \end{bmatrix} \tag{23}$$

and is introduced in order to allow sampling out from the structural state the actually observed (full-order) variables. Although the presence of $\boldsymbol{C}$ entails an additional computational burden, matrix multiplication $\boldsymbol{HC}$ can be carried out once and for all at the end of training, when $\boldsymbol{\Phi}_l$ has attained convergence.

## 3. JOINT ESTIMATION OF ROM STATE AND PARAMETERS

### 3.1. Joint estimation for time-invariant damage states

Having established the equations governing the reduced-order representation of the evolution of a partially observed structural system, we now move to the model identification task. We first consider the case of an undamaged structure, or of a damaged one characterized by a time-invariant damage state. Accordingly, the stiffness and damping matrices do not vary in the on-line stage of the analysis following the training; further to that, the POMs already established do not have to be updated if the envisioned kind of external loading does not change in time.

Within a stochastic frame we assume that the structural properties of the model are known only up to a certain degree of fidelity, or in other terms that they are (partially) unknown and must be estimated. The evolution and observation equations (19)-(20) are therefore rearranged as:

$$\boldsymbol{x}_{r,k} = \boldsymbol{f}_{r,k}\left(\boldsymbol{x}_{r,k-1}, \boldsymbol{\mathcal{F}}_{l,k}\right) + \boldsymbol{v}_k \tag{24}$$

$$\boldsymbol{y}_k = \boldsymbol{H}\boldsymbol{L}\,\boldsymbol{x}_{r,k} + \boldsymbol{w}_k \tag{25}$$

where: the augmented state vector $\boldsymbol{x}_{r,k} = [\,\boldsymbol{z}_{r,k} \quad \boldsymbol{\theta}_k]^{\mathrm{T}}$ collects both the state $\boldsymbol{z}_{r,k}$ of the ROM and the parameters $\boldsymbol{\theta}_k$ linked to the unknown features of the structural system; matrix $\boldsymbol{L} = [\boldsymbol{C} \quad \boldsymbol{0}]$ is used in place of $\boldsymbol{C}$ to account for the additional terms in the state vector $\boldsymbol{x}_{r,k}$ that cannot be physically observed; $\boldsymbol{f}_{r,k}$ is the nonlinear map within the current time step that describes the joint evolution of $\boldsymbol{z}_{r,k-1}$ and $\boldsymbol{\theta}_{k-1}$, based also on the random walk followed by model parameters; $\boldsymbol{v}_k$ and $\boldsymbol{w}_k$ respectively stand for the process and measurement noises, which are assumed to be zero mean white Gaussian processes with associated covariance matrices $\boldsymbol{V}$ and $\boldsymbol{W}$. The uncertainty term $\boldsymbol{v}_k$ is also due to the reduced accuracy of the ROM in comparison with the full-order counterpart; the relevant probability distribution was thoroughly investigated in [13], and shown to be far from providing a white noise term in the evolution equation in case of small $l$ values. In this study we anyway assume that standard assumptions of recursive Bayesian inference can be adopted. The uncertainty term $\boldsymbol{w}_k$ is instead related to the precision of the measurement devices, and can be reasonably assumed as a white Gaussian process.

The joint estimation of a partially observed system can be pursued through different techniques. In this work, two discrete Bayesian filters are compared: the extended Kalman filter (EKF), and the hybrid extended Kalman particle filter (EF-PF). The former one has been already discussed in [8] and is here reported in appendix A for a time-varying damage state to be discussed next; in what follows we specifically focus on the EK-PF approach only, trying to highlight its strengths and weaknesses. Dealing with joint estimation problems, the inherent nonlinearities of mapping $\boldsymbol{f}_{r,k}$ in Eq. (24) are know to become a potential source of filter instability, resulting in divergent or, even worse, biased estimates, see e.g. [35-37]. Since we handle a linear full-order structural model within each time step, such filter instability issues are seldom encountered, see [38, 39] for a theoretical analysis. Therefore, the use of alternative, more stable procedures like, e.g. the unscented Kalman filter [40] and Gaussian mixture algorithms [41], does not look compulsory for the situation under study. It would be rather different in the case of damage growth leading by itself to instability or failure of the structural system, or in the case of parameters of the constitutive model describing damage evolution to be tuned on-line. In the literature it has been already reported that, in such cases, the EKF may loose any capability to provide feasible estimates [8]. Since the same linearization scheme is adopted for the EKF and for the hybrid EK-PF, the same kind of instability-induced issues may be encountered. On the other hand, as pointed out in [10] for the nonlinear dynamics of simple systems, the superior performance of the EK-PF over a standard PF allows to largely reduce the number of particles to handle and so the computational costs. Since this latter feature looks particularly appealing for the framework here presented, wherein a ROM of the structure is continuously updated to obtain a real time detection of damage, issues related to the aforementioned linearization step of the filter are considered as possible negative side effects and checked not to spoil the solution. Further details on other filtering procedures can be found, e.g. in [11].

To deal with general problems, not necessarily featuring Gaussian probability distributions of the state variables in $\boldsymbol{x}_{r,k}$, sequential Monte Carlo methods can be adopted, see e.g. [42]. Such methods make no explicit assumptions concerning the probability distribution type, and

approximate the Chapman-Kolmogorov integrals behind the prediction stage of the filtering procedures through finite sums, adopting a sequential importance sampling over an adaptive stochastic grid. With particle filtering, a set of particles $\boldsymbol{x}_{r,k}^{i}$, with $i = 1, \dots, N_P$, supposed to be drawn from the (yet unknown) posterior distribution, is used to map the integrals. The estimate of $\boldsymbol{x}_{r,k}$ is next provided by weighting the contributions of all the particles, that have evolved according to the real dynamics of the system. Hence, no approximations linked to linearizations, or truncations of a Taylor series expansion of the evolution equation need to be introduced at this stage; as the particles sample the probability distribution to be computed, the approximation rests instead on substituting such unknown distribution with an arbitrarily chosen one, called importance function. Although mathematical details are not provided here for the sake of brevity, it must be noted that unbiased estimates have to be guaranteed, see [43]. The associated evolution of the weights $\omega_k^i$ adopted to finally merge the information conveyed by all the particles are so computed through [44]:

$$\omega_k^i = \frac{p(\boldsymbol{y}_{1:k}|\boldsymbol{x}_{r,0:k}^i)p(\boldsymbol{x}_{r,0:k}^i)}{\pi(\boldsymbol{x}_{r,k}^i|\boldsymbol{y}_{1:k})} \tag{26}$$

and subsequently normalized. In Eq. (26): $p(\boldsymbol{y}_{1:k}|\boldsymbol{x}_{r,0:k}^i)$ is the conditional probability density function (PDF) of the observation for a given state, which is often linked to the observation errors; $p(\boldsymbol{x}_{r,0:k}^i)$ is PDF of the system state; $\pi(\boldsymbol{x}_{r,k}^i|\boldsymbol{y}_{1:k})$ is the aforementioned importance function. Allowing also for the properties of Markov processes and for the obvious fact that the current state cannot depend on future observations, which are assumed conditionally independent, the recursive formula for the update of weights becomes, see [43, 45]:

$$\omega_k^i = \omega_{k-1}^i p(\boldsymbol{y}_k|\boldsymbol{x}_{r,k}^i) \tag{27}$$

In [46], it was shown that the variance of these weights increases stochastically over time: after a few time steps, one of the normalized weights tends to one, while all the remaining ones tend to zero. To address this rapid degeneracy phenomenon, a resampling stage may be used to eliminate samples with low importance weights and duplicate samples with high weights. Resampling somehow allows the filter to condense the cloud of particles around the peak probability zone(s), see [44]. If the systematic resampling scheme is adopted, see [47], this stage is performed by drawing a random sample $\zeta_j$ from the uniform distribution over the interval $(0,1]$; next, a generic $M$-th particle is duplicated if $\zeta_j$ is bounded by the values of the empirical cumulative distribution related to the $M-1$-th and the $M$-th particles, see [48].

As the dimension of the state vector increases, the computational costs associated with this procedure increase drastically, see [49]. To alleviate this issue still using the same sampling distribution, the quality of the ensemble of samples must be improved. Once the samples are drawn, they are pushed by an EKF toward the zones of higher probability, in order to better incorporate data from the latest observations.

Table  provides all the steps of this EK-PF strategy, where: the index $i$ is adopted for the current values of state covariance matrix $\boldsymbol{P}_k^i$ and Kalman gain $\boldsymbol{G}_k^i$, as they become particle-dependent too; a hat denotes the estimate provided by the filter at the end of the time step, or the initial guess at time $t_0$; $\mathbb{E}$ stands for expected value; $\boldsymbol{F}_{r,k}$ denotes the Jacobian of mapping $\boldsymbol{f}_{r,k}$ computed at $\widehat{\boldsymbol{x}}_{r,k-1}$, as before in accordance with the adopted explicit time integration procedure. If compared to a standard particle filter approach, this filtering scheme allows to dramatically reduce the number $N_\mathrm{P}$ of particles to handle in order to attain a given accuracy of the estimates; this is obtained with the additional burden of computing the Jacobian $\boldsymbol{F}_{r,k}$ at each time step. In the specific case of structural dynamics, it has been already shown that the additional EKF-driven step of the prediction stage, which comes along with the computation of the Jacobian $\boldsymbol{F}_{r,k}$ and with all the relevant matrix products listed in the same step of Table 1, may allow reducing by orders of magnitude the number $N_\mathrm{P}$ of samples necessary to attain the required accuracy of the estimations, see [10].

Table 1: the EK-PF algorithm for time-invariant damage states

- Initialization at time $t_0$, for $i = 1, \dots, N_\mathrm{P}$:

$$\widehat{\boldsymbol{x}}_{r,0} = \mathbb{E}[\boldsymbol{x}_{r,0}] \qquad \boldsymbol{x}_{r,0}^i = \widehat{\boldsymbol{x}}_{r,0}$$
$$\boldsymbol{P}_0 = \mathbb{E}\left[(\boldsymbol{x}_{r,0} - \widehat{\boldsymbol{x}}_{r,0})(\boldsymbol{x}_{r,0} - \widehat{\boldsymbol{x}}_{r,0})^\mathrm{T}\right] \qquad \omega_0^i = p(\boldsymbol{y}_0|\boldsymbol{x}_{r,0})$$

- At time $t_k$, for $k = 1, \dots, N_t$ and $i = 1, \dots, N_\mathrm{P}$:
  - Prediction stage:
    1. Draw particles:
$$\boldsymbol{x}_{r,k}^i \sim p(\boldsymbol{x}_{r,k}|\boldsymbol{x}_{r,k-1}^i)$$
    2. Push the particles toward the region of high probability through an EKF:
$$\boldsymbol{P}_k^{i-} = \boldsymbol{F}_{r,k}\boldsymbol{P}_{k-1}^i\boldsymbol{F}_{r,k}^\mathrm{T} + \boldsymbol{V}$$
$$\boldsymbol{G}_k^i = \boldsymbol{P}_k^{i-}\boldsymbol{L}^\mathrm{T}\boldsymbol{H}^\mathrm{T}\left(\boldsymbol{H}\boldsymbol{L}\boldsymbol{P}_k^{i-}\boldsymbol{L}^\mathrm{T}\boldsymbol{H}^\mathrm{T} + \boldsymbol{W}\right)^{-1}$$
$$\boldsymbol{x}_{r,k}^i = \boldsymbol{x}_{r,k}^{i-} + \boldsymbol{G}_k^i\left(\boldsymbol{y}_k - \boldsymbol{H}\boldsymbol{L}\boldsymbol{x}_{r,k}^{i-}\right)$$
$$\boldsymbol{P}_k^i = \boldsymbol{P}_k^{i-} - \boldsymbol{G}_k^i\boldsymbol{H}\boldsymbol{L}\boldsymbol{P}_k^{i-}$$
  - Update stage:
    1. Evolve weights:
$$\omega_k^i = \omega_{k-1}^i\, p(\boldsymbol{y}_k|\boldsymbol{x}_{r,k}^i)$$
    2. Systematic resampling, for $j = 1, \dots, N_P$:
       - draw a random sample $\zeta_j$ from uniform distribution over $(0, 1]$
       - find $M$ that satisfies:
$$\sum_{i=1}^{M-1}\omega_k^i < \zeta_j \le \sum_{i=1}^{M}\omega_k^i$$
       - $\boldsymbol{x}_{r,k}^j \leftarrow \boldsymbol{x}_{r,k}^M$
    3. Compute expected value (and other required statistics):
$$\widehat{\boldsymbol{x}}_{r,k} = \sum_{i=1}^{N_\mathrm{P}}\omega_k^i\boldsymbol{x}_{r,k}^i$$

## 3.2. Joint estimation for time-varying damage states

At variance with the former case, since damage evolves and the characteristics of the response of the structure to the external loads change as well, the ROM needs to be re-trained while the damage itself is identified. To purposely avoid a time consuming re-training stage whenever damage evolves, so potentially within each time window between two subsequent observations, the same observations can be exploited to tune the already available POMs. In fact, according to the introduced principle of time-scale separation (applicable when damage grows with a dynamics much slower than the structural system's one) we can assume that POMs slowly evolve, and the (supposed small) differences between their shapes at the beginning and at the end of each time step can be tracked with the use of a KF. Whenever the output of the ROM shows a degraded capability to match the response of the observed structure, instead of moving back to the full-order model, updating the damage state on the basis of any available forecast and finally training a new ROM, in this study we only adjust the shapes of the handled POMs and simultaneously foresee damage evolution. This additional last task has therefore to be trackled by further enlarging the set of variables to be estimated online by the filters. Within the proposed frame, the joint estimation problem thus consists in tracking the

ROM state, estimating the unknown system parameters and then online updating the damage-related subspace of the ROM.

Like for the time-invariant case, the EK-PF can be used for the standard joint estimation task; besides this, an ad-hoc KF is used for the update of the subspace initially provided by POD, in terms of the retained POMs. The iterative procedure is initialized at time $t_0$ also in terms of an initial guess of the POMs, whose shapes are provided from the previous offline training stage carried out for the healthy structure, or for the structure assumed to be characterized by a non-evolving damage state. Within a stochastic environment, the variability of POM components induced by damage has to be estimated too, in order to later allow the KF to track the POMs in real-time or, at least, with minimal delay.

Within the time step $[t_{k-1}\ \ t_k]$, the state-space model now reads:

$$\boldsymbol{x}_{r,k} = \boldsymbol{f}_{r,k}\left(\boldsymbol{x}_{r,k-1}, \boldsymbol{\mathcal{F}}_{l,k}\right) + \ \boldsymbol{v}_k \tag{28}$$

$$\boldsymbol{y}_k = \boldsymbol{H}\boldsymbol{L}_k\, \boldsymbol{x}_{r,k}\ + \boldsymbol{w}_k \tag{29}$$

where the index $k$ is used also for the $\boldsymbol{L}$ matrix, as POMs $\boldsymbol{\Phi}_{l,k}$ have to be tracked and may continuously change in time.

To handle ROM updating, all the POMs are arranged in vector form according to, see [20, 27]:

$$\boldsymbol{\varphi}_{l,k} = \begin{bmatrix} \boldsymbol{\Phi}_{1,k} \\ \vdots \\ \boldsymbol{\Phi}_{l,k} \end{bmatrix} \tag{30}$$

and their evolution is modelled as a random walk:

$$\boldsymbol{\varphi}_{l,k} = \boldsymbol{\varphi}_{l,k-1} + \boldsymbol{\varsigma}_k \tag{31}$$

where $\boldsymbol{\varsigma}_k$ is a purposely introduced zero mean, white Gaussian noise with covariance matrix $\boldsymbol{\Upsilon}$.

As for any filtering/identification procedure, POMs can be tracked if observations are exploited. A further observation equation is thus introduced along with the evolution equation (31), and it reads:

$$\boldsymbol{y}_k = \boldsymbol{H}_{ss}\boldsymbol{\varphi}_{l,k} + \boldsymbol{w}_k \tag{32}$$

where: $\boldsymbol{H}_{ss}$ (where index $ss$ stands for subspace) is a stationary matrix used to link observables to the subspace spanned by POMs; $\boldsymbol{w}_k$ still accounts for measurement uncertainties, since vector $\boldsymbol{y}_k$ is the same handled in Eq. (29). Eq. (32) is accordingly a different way of representing the link between the observations and the varying ROM state, since the equations governing structural dynamics are the same furnished by the ROM.

Table 2: the EK-PF-KF algorithm for time-varying damage states

- Initialization at time $t_0$, for $i = 1, \dots, N_{\mathrm{P}}$:

$$\widehat{\boldsymbol{x}}_{r,0} = \mathbb{E}\left[\boldsymbol{x}_{r,0}\right] \qquad \boldsymbol{x}_{r,0}^{i} = \widehat{\boldsymbol{x}}_{r,0}$$
$$\boldsymbol{P}_0 = \mathbb{E}\left[\left(\boldsymbol{x}_{r,0} - \widehat{\boldsymbol{x}}_{r,0}\right)\left(\boldsymbol{x}_{r,0} - \widehat{\boldsymbol{x}}_{r,0}\right)^{\mathrm{T}}\right] \qquad \omega_0^{i} = p\left(\boldsymbol{y}_0 | \boldsymbol{x}_{r,0}\right)$$
$$\widehat{\boldsymbol{\varphi}}_{l,0} = \mathbb{E}\left[\boldsymbol{\varphi}_{l,0}\right] \qquad \boldsymbol{P}_{ss,0} = \mathbb{E}\left[\left(\boldsymbol{\varphi}_{l,0} - \widehat{\boldsymbol{\varphi}}_{l,0}\right)\left(\boldsymbol{\varphi}_{l,0} - \widehat{\boldsymbol{\varphi}}_{l,0}\right)^{\mathrm{T}}\right]$$

- At time $t_k$, for $k = 1, \dots, N_t$ and $i = 1, \dots, N_{\mathrm{P}}$:
  - Prediction stage:
    1. Draw particles:

$$\boldsymbol{x}_{r,k}^{i} \sim p\left(\boldsymbol{x}_{r,k} | \boldsymbol{x}_{r,k-1}^{i}\right)$$

    2. Push the particles toward the region of high probability through an EKF:

$$\boldsymbol{P}_k^{i-} = \boldsymbol{F}_{r,k} \boldsymbol{P}_{k-1}^{i} \boldsymbol{F}_{r,k}^{\mathrm{T}} + \boldsymbol{V}$$
$$\boldsymbol{G}_k^{i} = \boldsymbol{P}_k^{i-} \boldsymbol{L}_{k-1}^{\mathrm{T}} \boldsymbol{H}^{\mathrm{T}} \left(\boldsymbol{H} \boldsymbol{L}_{k-1} \boldsymbol{P}_k^{i-} \boldsymbol{L}_{k-1}^{\mathrm{T}} \boldsymbol{H}^{\mathrm{T}} + \boldsymbol{W}\right)^{-1}$$

$$\boldsymbol{x}_{r,k}^{i} = \boldsymbol{x}_{r,k}^{i-} + \boldsymbol{G}_k^{i} \left(\boldsymbol{y}_k - \boldsymbol{H} \boldsymbol{L}_{k-1} \boldsymbol{x}_{r,k}^{i-}\right)$$
$$\boldsymbol{P}_k^{i} = \boldsymbol{P}_k^{i-} - \boldsymbol{G}_k^{i} \boldsymbol{H} \boldsymbol{L}_{k-1} \boldsymbol{P}_k^{i-}$$

    3. Evolve subspace and predict covariance:

$$\boldsymbol{\varphi}_{l,k}^{-} = \boldsymbol{\varphi}_{l,k-1}$$
$$\boldsymbol{P}_{ss,k}^{-} = \boldsymbol{P}_{ss,k-1} + \boldsymbol{\Upsilon}$$

  - Update stage:
    1. Evolve weights:

$$\omega_k^{i} = \omega_{k-1}^{i}\, p\left(\boldsymbol{y}_k | \boldsymbol{x}_{r,k}^{i}\right)$$

    2. Systematic resampling, for $j = 1, \dots, N_P$:
       - draw a random sample $\zeta_j$ from uniform distribution over $(0, 1]$
       - find $M$ that satisfies:

$$\sum_{i=1}^{M-1} \omega_k^{i} < \zeta_j \leq \sum_{i=1}^{M} \omega_k^{i}$$

       - $\boldsymbol{x}_{r,k}^{j} \leftarrow \boldsymbol{x}_{r,k}^{M}$
    3. Compute expected value (and other required statistics):

$$\widehat{\boldsymbol{x}}_{r,k} = \sum_{i=1}^{N_{\mathrm{P}}} \omega_k^{i} \boldsymbol{x}_{r,k}^{i}$$

    4. Compute subspace Kalman gain:

$$\boldsymbol{G}_{ss,k} = \boldsymbol{P}_{ss,k}^{-} \boldsymbol{H}_{ss}^{\mathrm{T}} \left(\boldsymbol{H}_{ss} \boldsymbol{P}_{ss,k}^{-} \boldsymbol{H}_{ss}^{\mathrm{T}} + \boldsymbol{W}\right)^{-1}$$

    5. Update subspace and covariance:

$$\boldsymbol{\varphi}_{l,k} = \boldsymbol{\varphi}_{l,k}^{-} + \boldsymbol{G}_{ss,k} \left(\boldsymbol{y}_k - \boldsymbol{H}_{ss} \boldsymbol{\varphi}_{l,k}^{-}\right)$$
$$\boldsymbol{P}_{ss,k} = \boldsymbol{P}_{ss,k}^{-} - \boldsymbol{G}_{ss,k} \boldsymbol{H}_{ss} \boldsymbol{P}_{ss,k}^{-}$$

Eqs. (31) and (32) respectively provide a linear time evolution for the POMs, and a linear relationship between the observation vector $\boldsymbol{y}_k$ and the subspace $\boldsymbol{\varphi}_{l,k}$: so, a KF (which is an optimal estimator for linear state-space models) can be used for the online update of the subspace. The joint estimation algorithm discussed for the time-invariant case is accordingly modified as reported in **Error! Reference source not found.**, where account has been taken of the variability of POMs during the two stages of filtering. For the sake of completeness and to also provide a clear comparison between the EF-PF-KF procedure here considered and the EKF-KF one already proposed in [20], the latter approach is briefly described in Appendix A.

Since the KF is run in parallel with the EK-PF, and matrix $\boldsymbol{L}_k$ and vector $\boldsymbol{\varphi}_{l,k}$ are to be continuously updated, a step-by-step linearization has to be properly designed to compute $\boldsymbol{F}_{r,k}$ at step 2 of the prediction stage. In the proposed approach, we adopt again a purely explicit linearization and allow for POMs updated up to time $t_{k-1}$, as collected in matrix $\boldsymbol{L}_{k-1}$. Possible effects of estmation time delays are again supposed to be marginal in the present context, since $\Delta t$ is bounded from above by structural vibrations. With the proposed algorithm, the further update step is centered on the computation of the Kalman gain $\boldsymbol{G}_{ss,k}$, which then drives the online tracking of all the POMs in $\boldsymbol{\varphi}_{l,k}$.

## 4. NUMERICAL RESULTS

In this Section, simulated experiments are used to validate the proposed methodology. In doing so, results are provided for the shear building considered in [22], see also [20]: this structure consists of eight storys, with floor mass of $625$ t and interstory stiffness of $10^6$ kN/m. To make the model more realistic, the values of the floor masses and of the interstory stiffnesses were randomized by adding a scattering characterized by a standard deviation of $5\%$ of the aforementioned values for masses and stiffnesses. As far as damping is concerned, in [22] a non-classical one was allowed for; here, following [20], a standard Rayleigh damping ($\boldsymbol{D} = a\,\boldsymbol{M} + b\,\boldsymbol{K}$) with a $2\%$ ratio for the first two structural modes is instead assumed. To provide an overview on the dynamic characteristics of the structure, the relevant undamped vibration frequencies are collected in Table .

Althoug in [20] it has been shown that, for the structural models adopted for shear type buildings under a non-stationary excitation, ROM features are slightly depedent on the excitation itself, the results gathered in this study have been obtained by exciting the system with a harmonic force $F = 5 \cdot 10^7 \sin(30\pi t)$ applied to the top floor. The outcomes to be discussed next can be easily generalized to allow for multiple non-stationary input loadings; anyhow, this generalization would not increase the complexity and capability of the proposed identification procedure, provided that loading features can be conveyed into the initial full-order model, see e.g. [50]. To avoid issues related to the identifiability of damage in case of damped vibrations, see e.g. [35], if not otherwise stated the load is assumed to act on the structure for the entire duration of the analysis.

Pseudo-experimental data have been generated to mimic real system observations collected at all the floors. Results of a direct analysis, in terms of lateral story displacements, have been thus corrupted with an uncorrelated zero mean Gaussian noise featuring a reference value of 1 mm for the relevant standard deviation. This level of precision could be obtained by interferometric radars (e.g. see [51]) or, alternatively, by dual frequency GPS sensors [52]. The

algorithm can also perform rather well with higher noise levels, as shown in what follows, however an increase in the noise level can deteriorate the convergence rate of the filtering scheme.

Before moving to the analysis of method performance when a ROM is handled, in Section 4.1 the outcomes of the EK-PF and of the EKF are compared in terms of system identification. To also get further insights into the efficiency of the EK-PF, when compared to a standard PF, results relevant to this latter filtering approach are also included. Two model classes are considered: a first one featuring 1 unknown stiffness parameter only, and another one featuring all the interstory parameters unknown. It is shown that EKF and EK-PF outperform the PF when dealing with the former model class. Subsequently, EK-PF and EKF are applied to system identification of the latter model class, and it is observed that an increase in model complexity adversely affects their performances, with the EK-PF providing marginal advantage over the EKF. In Section 4.2, the performances of EK-PF and EKF are then compared for system identification of a single DOF ROM of the case study.

Table 3: undamped vibration frequencies of the 8-story shear building

| Mode | frequency (Hz) |
|---|---|
| 1 | 1.187 |
| 2 | 3.481 |
| 3 | 5.678 |
| 4 | 7.734 |
| 5 | 9.434 |
| 6 | 10.920 |
| 7 | 11.910 |
| 8 | 12.647 |

## 4.1 Full-order model of a shear building: system identification

As anticipated, we first benchmark the EK-PF-KF approach against the alternate EKF-KF one and a simplified PF-KF method, which does not require the computation of the state mapping gradient in the prediction stage. To assess the effects of filters' tuning parameters on estimation accuracy and rate of convergence towards steady-state solutions, the stage of updating of the ROM is deactivated: hence, for a time-invariant damage state (e.g. the virgin one), we attack the problem by handling the full-order model of the structure.

Two different problems or model classes are considered. The first one handles the interstory stiffnesses all featuring the same value; besides this parameter, also the two Raleigh damping coefficients $a$ and $b$ need to be estimated. The second one handles instead the interstory stiffnesses independently; therefore, the number of the unknown parameters to be estimated grows to 8. To catch the effects of damping on the structural response, the harmonic load applied to the top floor is assumed to get stopped at $t = 25$ s.

In the analyses, the covariance matrices relevant to the state process noise and to the initial guess are respectively set as $\mathbf{V} = 10^{-20}\boldsymbol{I}$ and $\mathbf{P}_0 = 10^{-20}\boldsymbol{I}$, where $\boldsymbol{I}$ stands for the identity matrix; the said values represent the magnitudes of the diagonal entries corresponding to displacements, velocities and accelerations, so the relevant measurement units are respectively $m^2$, $(m/s)^2$ and $(m/s^2)^2$. The pivotal entries of the other process and tuning noise matrices,

relevant to the interstory stiffness $k$ and to the damping coefficients $a$ and $b$, are reported in Table 4 for the three procedures adopted.

In Figure 1 the corresponding results of parameter estimation are presented and compared. In the analysis, the values of $\mathrm{V}^k$ and $\mathrm{P}_0^k$ terms reported in Table 4 have been adopted. The time evolution of each estimate is given in a nondimensional form, namely as the ratio between the current value furnished by the filter and the target value; accordingly, with this representation all the plots have to converge to 1 to testify the accuracy of the results. To also assess the possible effect of the initialization on the filters' performance, evolutions departing from two different starting values at $t = 0$ are reported; similar trends are provided by other initial guesses, but are not shown in the graphs. It can be observed that the three methods can estimate $k$ with a good accuracy. However, although difficult to see at the graph scale, the estimates related to EKF and EK-PF are more stable in the final stage of the analysis, when the vibrations are damped; some (small) fluctuations show up instead in the time evolution provided by the PF. Regarding the two damping coefficients, when the initial guess for $a$ is larger than the target value, the EKF and EK-PF provide again accurate estimates of both of them; the other way around, when the initial guess for $a$ is smaller than the target, a bias is found in the relevant steady-state solution while $b$ is still estimated correctly. It must be remarked that, in the forced vibrations stage of the analysis, the damping parameters are not identifiable by any method; this is linked to low sensitivity of the response to variations in $a$ and $b$ in this initial phase. After $t = 25$ s, when the loading is stopped and the structural vibrations are progressively damped out, the estimates of $a$ and $b$ soon converge towards the aforementioned asymptotic solutions.

It should be also highlighted that only $N_\mathrm{P} = 100$ particles have been handled with the EK-PF, whereas $N_\mathrm{P} = 2000$ particles have been generated at each recursion of the PF. Hence, the EK-PF outperforms the PF not only in terms of accuracy but also of computational effort. Similar performaces are obtained for higher noise levels, and relevant results are here omitted for the sake of brevity.

Table 4: full-order model class 1: pivotal covariance values for the parameters $k$, $a$ and $b$ to be estimated, and for the three adopted filtering procedures.

| | $\mathrm{V}^k$ (MPa$^2$) | $\mathrm{V}^a$ | $\mathrm{V}^b$ | $\mathrm{P}_0^k$ (MPa$^2$) | $\mathrm{P}_0^a$ | $\mathrm{P}_0^b$ |
|---|---|---|---|---|---|---|
| EKF | $10^9$ | $10^{-11}$ | $10^{-10}$ | $10^{15}$ | $10^{-9}$ | $10^{-7}$ |
| PF | $10^{12}$ | $10^{-10}$ | $10^{-8}$ | $10^{15}$ | $10^{-8}$ | $10^{-6}$ |
| EK-PF | $10^{11}$ | $10^{-9}$ | $10^{-8}$ | $10^{15}$ | $10^{-10}$ | $10^{-6}$ |

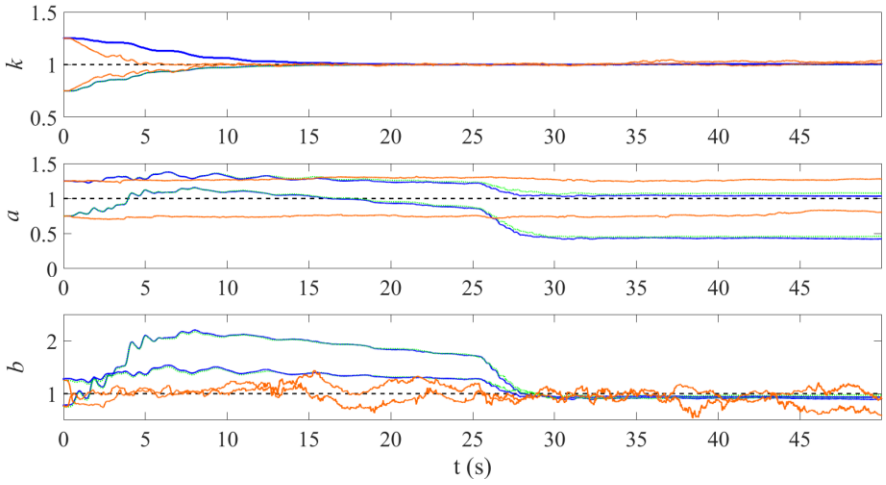


Figure 1: full-order model class 1: comparison among the estimated (continuous lines) non-dimensional time evolutions of model parameters $k$, $a$ and $b$, obtained starting from two initializations and using the EK-PF (green lines), the EKF (blue lines), and the PF (orange lines).

As far as model class 2 is concerned, in Figure 2 the results of parameter identification provided by the EKF and EK-PF are presented for a noise level equal to 1 mm as for model class 1; the PF, which has already shown poor performance indices, is not considered any longer. At variance with the previous case and due to the number of unknown parameters to be estimated increased from 3 to 8, with the EK-PF method $N_P = 1000$ particles have been drawn; negligible improvements are displayed by increasing this value up to $N_P = 5000$. Graphs show that both filters lead to convergence to the target values, although the EK-PF features a faster convergence rate. In this case, for both EKF and EK-PF methods the covariances of parameter process noise and parameter initial guess were set $\mathbf{V}^{\boldsymbol{k}} = 10^{12}\boldsymbol{I}$ MPa$^2$ and $\mathbf{P}_0^{\boldsymbol{k}} = 10^{15}\boldsymbol{I}$ MPa$^2$, respectively. In Figure 3 the results of parameter estimation are presented for a value of the measurement standard deviation increased till 3 mm. Even if neither of the methods provides convergence to the target for the parameters, the solutions are always stable (namely, do not diverge) and are affected by a discrepancy amounting to around 25% at most, independently of the initialization values (though not shown in these graphs).

Overall, it can be concluded that the observation noise terms can lead to biased estimates of the parameters, and the issue is obviously more pronounced when dealing with structural models that feature a large set of unknowns. Next, a thorough parametric study is performed for a ROM of the case study and it is shown that, even for large noise to signal ratios, the identification is performed with a reasonable level of accuracy due to the reduced number of model parameters to be tuned.

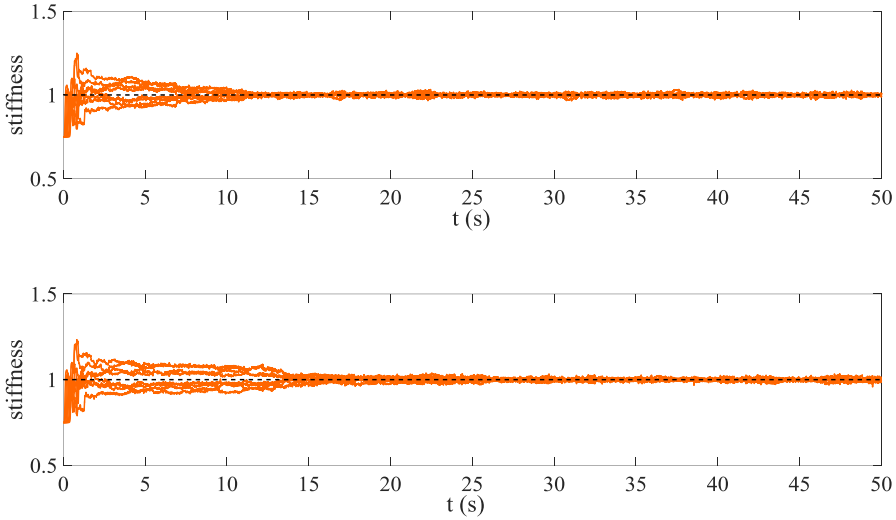


(a)




(b)

Figure 2: full-order model class 2, noise level equal to 1 mm: comparison between the estimated non-dimensional time evolutions of the stiffness terms, obtained using (a) the EK-PF, and (b) the EKF.

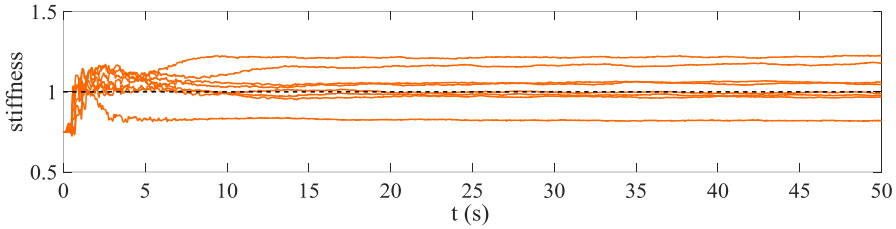


(a)

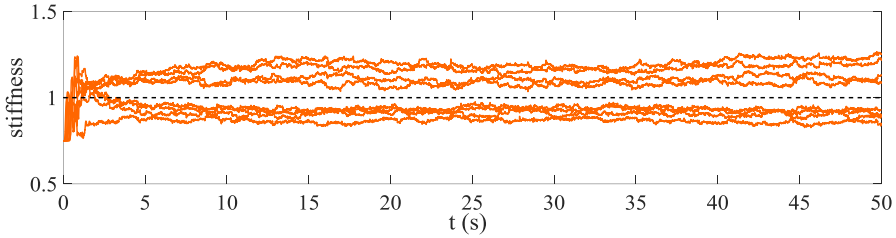


(b)

Figure 3: full-order model class 2, noise level equal to 3 mm: comparison between the estimated non-dimensional time evolutions of the stiffness terms, obtained using (a) the EK-PF, and (b) the EKF.

## 4.2 Reduced-order model of a shear building: damage detection and ROM update

Allowing for the results of Section 4.1, the PF-based approach is not considered when handling a ROM of the structure. Accordingly, to assess the capability of the proposed EK-PF-KF approach, a comparison is made again with the EKF-KF method given in [20].

A time-varying damage state is now allowed for. The damage itself is assumed to be induced by effects not explicitly covered by the considered equation of motion; hence, stiffness degradation is not induced by the harmonic force $F$ applied to the top floor. Although unknown during the filtering procedure, damage consists in the following sequence of piece-wise (time) constant reduction by $50\%$ (or $25\%$ in the last case considered in this Section) of the original (undamaged) interstory stiffness terms: at $t = 180$ s, at the story #1 level; at $t = 240$ s, at the story #8 level; at $t = 300$ s, at the story #3 level; at $t = 360$ s, at the story #7 level.

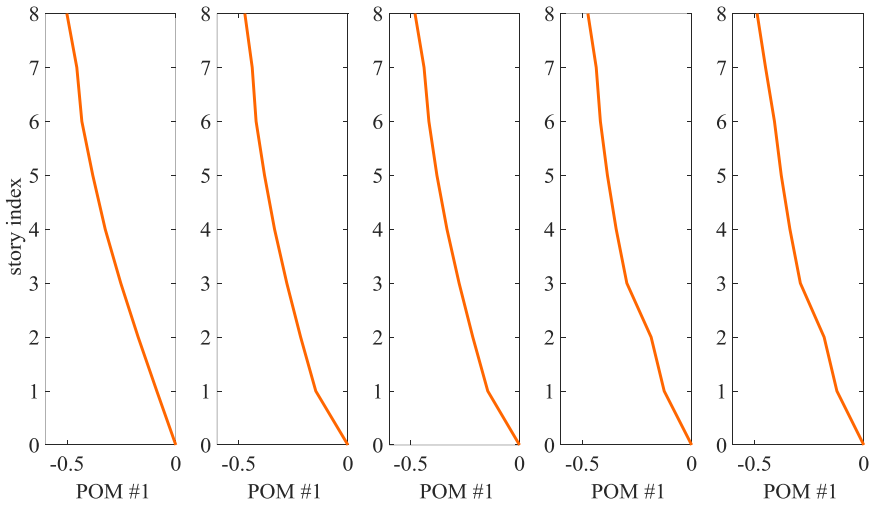


Figure 4: from left to right, target POM shapes for the healthy state and at each of the four stages of damage growth, for $50\%$ damage events.

In all the analyses to follow, we set that only one POM is retained in the ROM, i.e. that $l = 1$ (see Section 2); the relevant minimum accuracy of the model accordingly gets $p = 0.8 - 0.9$, see Eq. (17), depending on the damage stage. The shapes of the POM for the healthy state and for each stage of damage growth are all reported in Figure 4. For different settings, allowing for additional POMs retained in the ROM but with a time-invariant state of damage after its inception, readers are referred to [20]. As already remarked in [13, 20], whenever damage occurs a kink (or an additional kink) shows up in the fundamental vibration mode of the structure, which has been formerly smoother due to the properties of the structure. Because of the frequency of excitation and of the evolution of damage here considered, multiple kinks are shown by the POM shapes in Figure 4; therefore, a detection or identification of the damage location might not be a simple task, see also [27].

Concerning the identification task and its initialization, in all the analyses we have assumed to move from the former ROM training stage. Accordingly, $\widehat{\boldsymbol{\varphi}}_{l,0}$ (see Tables 2 and A.1) is the

trained POM at the beginning of SHM. Even if obtained from the said offline training stage and so optimized to track the actual system dynamics at $t = 0$, to allow for the uncertainties in the stiffness properties of the structural members the initial value $\boldsymbol{P}_{ss,0}$ of the covariance matrix is set to let each component of $\boldsymbol{\varphi}_l$ to subsequently vary, especially when the damage changes. Due to the intricate methodology here proposed, a robust and case-independent initialization of $\boldsymbol{P}_{ss}$ does not prove simple to establish; a trial-and-error method has thus provided a quasi-optimal solution as $\boldsymbol{P}_{ss,0} = 10^{-12}\boldsymbol{I}$ m$^2$. Matrix $\boldsymbol{\Upsilon}$, allowing instead for the effects of the Gaussian noise related to the ROM update, see Eq. (31), has been set as $\boldsymbol{\Upsilon} = 10^{-10}\boldsymbol{I}$ m$^2$. With the EKF-KF approach, vector $\hat{\boldsymbol{x}}_{r,0}$ is typically determined by considering the amplitude characteristics, at time $t = 0$, of the POM (or POMs in general) retained in the ROM, and of the target or design values of the unknown stiffness terms. As far as this latter aspect is concerned, a parametric analysis has been also performed to check the sensitivity of the proposed approach to the initial uncertainties in the stiffness properties of the structure; as discussed below, results are not shown here for brevity, but the method results to be quite insensitive to such uncertainty source at the system level. $\boldsymbol{P}_0$ has been accordingly set to allow a variation of all the variables in $\boldsymbol{x}_{r,k}$, keeping also in mind that the sub-vector $\boldsymbol{z}_{r,k}$, see Eq. (18), collects the model DOFs in the ROM sub-space with $\boldsymbol{\varphi}_{l,k}$ being normalized. More importantly, matrix $\boldsymbol{V}$ has to permit the stochastic variation of the components of $\boldsymbol{x}_{r,k}$, see **Error! Reference source not found.**, and has been therefore set diagonal, with pivotal entries relevant to $\boldsymbol{z}_{r,k}$ featuring a dimensionless amplitude on the order of $10^{-1} - 10^{-4}$, and with an entry relevant to the POM stiffness $\boldsymbol{\mathcal{K}}_l$ (which is actually a scalar in the present one-POM case) on the order of $10^{12}$ MPa$^2$. The same settings have been adopted also for the matrices shared with the EKF-KF approach. In the present work, the process and observation noise covariances are assumed a-priori known; however, in practical cases these covariances should be appropriately estimated to ensure that an optimal prediction is furnished by the filters, see [53, 54].

The number of particles adopted in the analyses has been set now to $N_\mathrm{P} = 100$, as marginal improvements have been displayed by increasing it up to $N_P = 2000$. Such small number of samples helps attaining a speedup (see below) when tracking the ROM dynamics instead of the full-order one; the other way around, some pollution or fluctuations are shown in the time evolution of the estimates provided, which can be somehow reduced by increasing $N_\mathrm{P}$.

The performance of the EKF-KF and EK-PF-KF procedures in tracking the shape evolution of the retained POM is reported in Figure 5, in terms of the estimated (and not trained or re-trained) solutions at the end of monitoring at $t = 600$ s. Due to the collected observations of each story displacement, both methods perform rather well and the only discrepancy shown, in comparison with the target solution, is actually induced by the considered measurement noise. The time evolution of the estimated POM is also depicted in Figure 6 for the exemplary EK-PF-KF case, starting at $t = 0$ from the initial shape foreseen for the healthy state; remarkably, although not explicitly shown, this time evolution is marginally affected by the initial guess concerning the structural properties to be estimated.

The estimated time evolutions of all the components of the POM, namely of all the lateral story displacements, are gathered in Figure 7. Even if the final estimations in Figure 5, relevant to $t = 600$ s, look similar and both of the same accuracy, these graphs show that the EK-PF-KF procedure reacts (slightly) faster than the EKF-KF one to the changes induced by the sudden drops of the stiffness terms, not necessarily leading to an increase of each components of the

POM. The solution provided by the filters looks polluted by fluctuations of small amplitude, possibly leading to instability and so divergence or biases in the estimates in the long term range. Such fluctuations, already shown in [10] and in [55] for a single DOF case, can be somehow reduced with the EK-PF-KF procedure by increasing the number $N_P$ of particles, so reducing the computational gain with respect to the full-order case. In these graphs, once again evolutions are provided for different initialization values for the POM components, so as to assess the robustness of the methods against possible initial inaccuracies related to the ROM state.

The reported incapability to match all the step-wise stiffness changes close to real-time, may also lead to biases in the estimates of the damage state or to a delay in the monitoring of drifts of the structural state. To address this issue, in Figure 8 a comparison is shown regarding the forecasted time variations of the unknown scalar ROM stiffness term computed according to Eq. (15), on the basis of the current estimate of the POM retained in the analysis. In each plot, the two time evolutions are related to initializations of the stiffness value affected by an error of $\pm 50\%$ with respect to the target one; besides the current estimate, also the corresponding 99% confidence interval is reported. As for the expected values, the two approaches lead to very similar trends, and the finally predicted values are both free from biases though the EK-PF-KF procedure shows a faster convergence rate each time the stiffness drops. Concerning the uncertainty level of estimations, the confidence interval provided by the EKF-KF approach never decreases in time, since it is continuously propelled by relevant terms in the covariance matrices, to allow appropriate stiffness variation anytime damage evolves. The very narrow confidence interval provided instead by the EK-PF-KF approach is primarily due to the beneficial effects of the EKF adopted in the prediction stage; the same trend was already shown in [10] right after this stage, whereas samples (and the corresponding parameter confidence intervals) were rather scattered before it, similarly to what reported for the EKF-KF case.

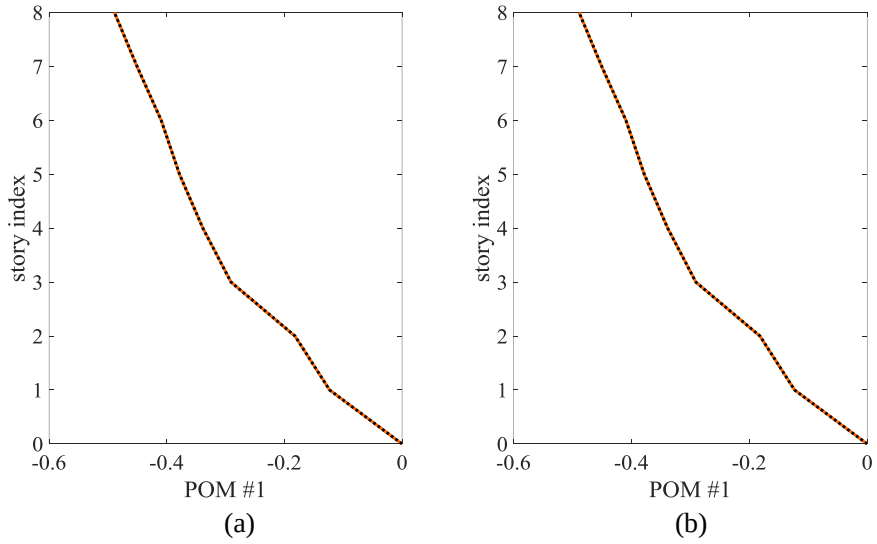


Figure 5: comparison between target (dashed lines) and estimated (continuous lines) POM shapes and at the end of monitoring. Results obtained for 50% damage events, with (a) the EKF-KF approach and (b) the EK-PF-KF approach.

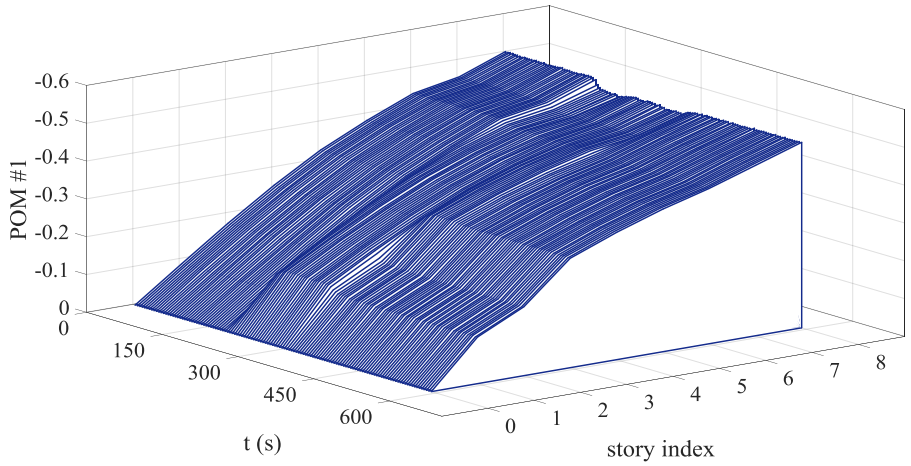


Figure 6: EK-PF-KF approach, 50% damage events, time evolution of the estimated POM shape.

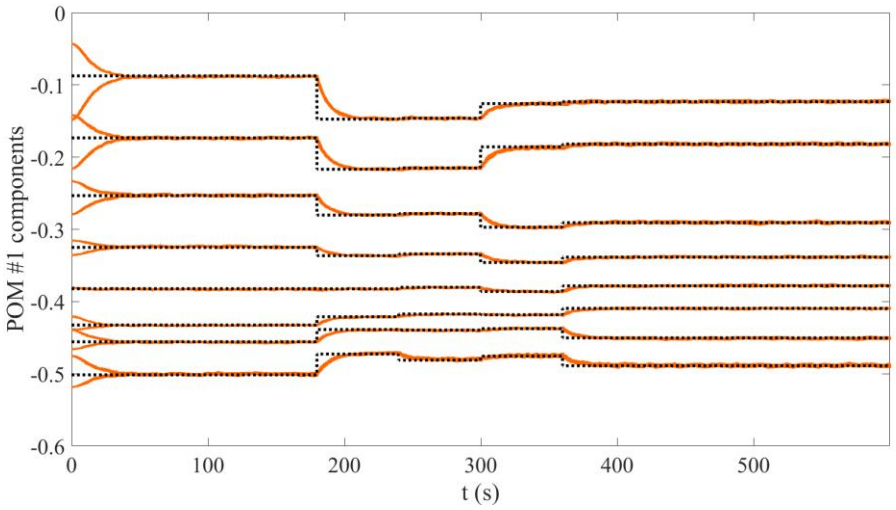


(a)

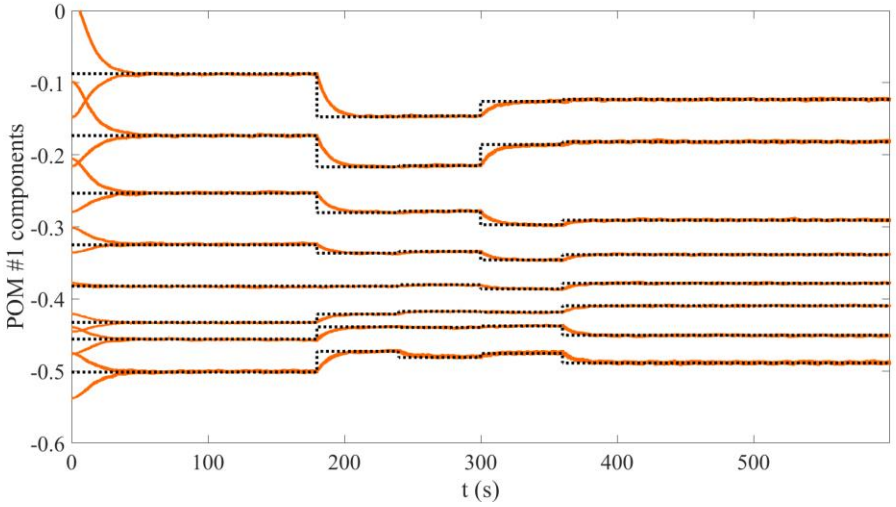


(b)

Figure 7: comparison between target (dashed lines) and estimated (continuous lines) time evolutions of POM components. Results obtained for 50% damage events,with (a) the EKF-KF approach and (b) the EK-PF-KF approach.

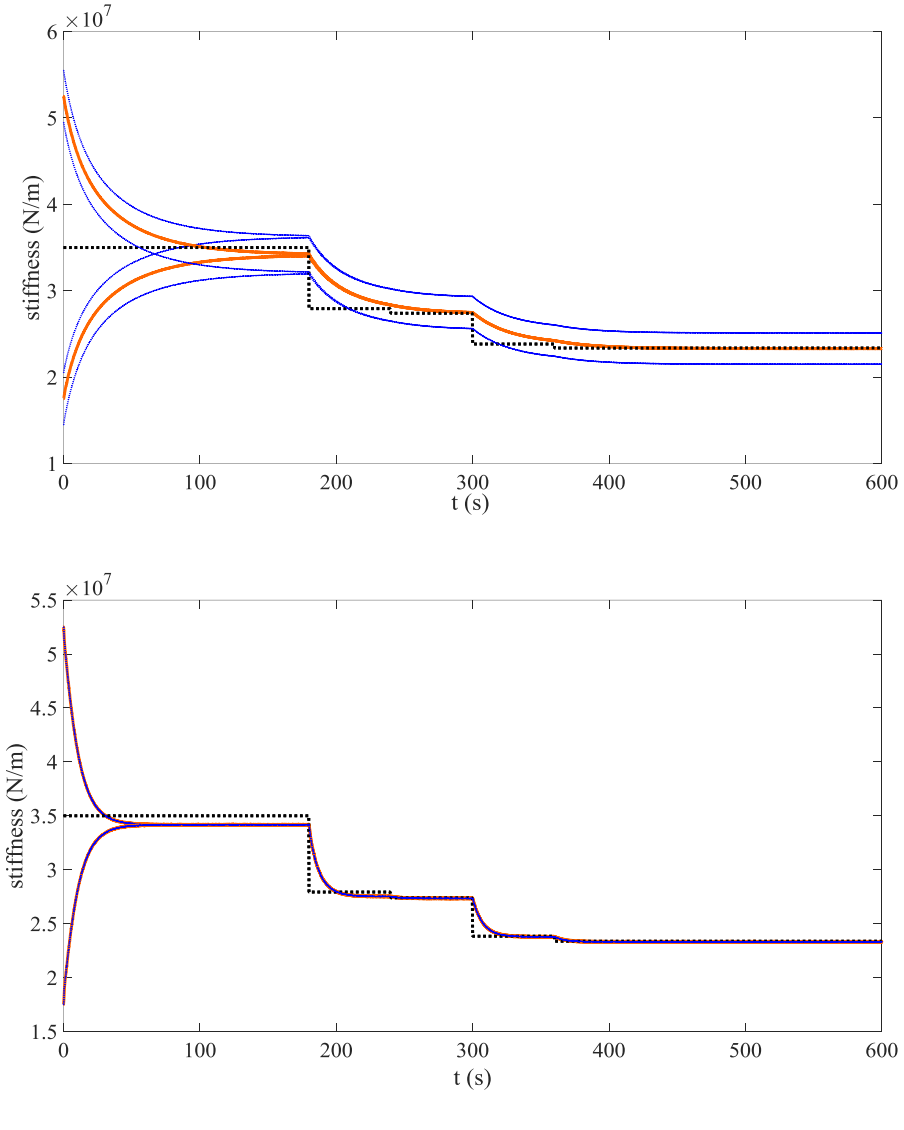


Figure 8: comparison between target (dashed lines) and estimated (continuous lines) time evolutions of the single-DOF MOR stiffness, and relevant 99% confidence intervals. Results obtained for 50% damage events, with (a) the EKF-KF approach and (b) the EK-PF-KF approach.

Some additional results are reported in Figure 9, in terms of the time evolutions of the tracked lateral story displacements compared to the target (noise-free) ones. Like for the identification/update tasks, it is shown that the two methodologies similarly perform. Story displacements are estimated without any drift or time delay, even if high frequency oscillations are obviously filtered out having considered one POM only in the analysis.

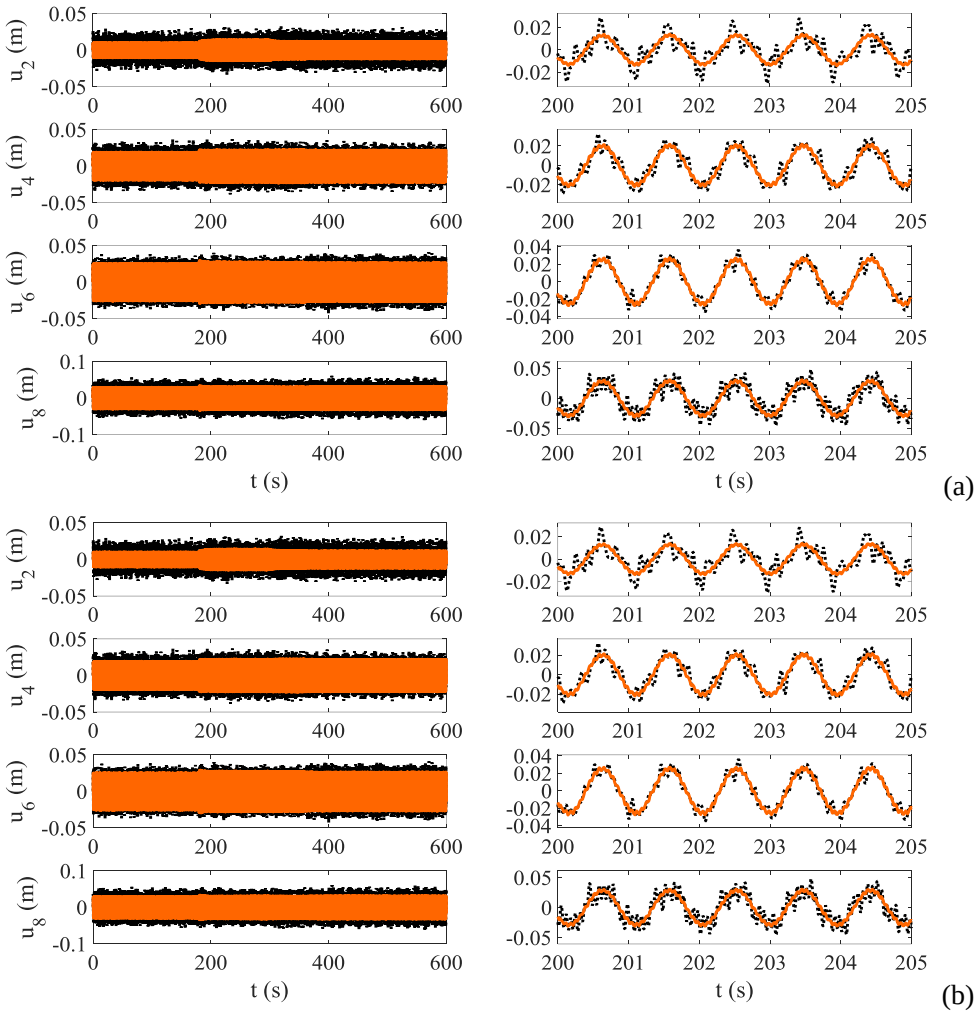


Figure 9: comparison between target (dashed lines) and estimated (continuous lines) time evolutions of the lateral displacements (from top to bottom) at stories 2,4,6, and 8. Results obtained for 50% damage events, with (a) the EKF-KF approach and (b) the EK-PF-KF approach; right panels provide close-up views of the results in the left panels, relevant to the whole monitoring phase.

The effect of the tuning noise for the subspace components on filter performance, as parametrized by $\boldsymbol{\Upsilon}$ (see Eq. (31) and the discussion to follow), is now investigated. In Figure 10, two settings respectively featuring $\boldsymbol{\Upsilon} = 10^{-9}\boldsymbol{I}$ m$^2$ and $\boldsymbol{\Upsilon} = 10^{-11}\boldsymbol{I}$ m$^2$ are cross-compared. While $\boldsymbol{\Upsilon}$ marginally affects parameter estimation, it can be seen that, as far as model update is concerned: a relatively smaler tuning noise can reduce the convergence rate of the filter; a relatively larger tuning noise can lead instead to estimates affected by a consistent degree of uncertainty.

To assess next the sensitivity of the proposed approach to the damage level, in Figure 11 the EK-PF-KF estimates of POM components and ROM stiffness variation for a case featuring a damage level of 25%, instead of the 50% considered so far, are gathered. It can be observed that the filter performance is not affected by the amount of damage. It is also worth stressing that these results have been obtained without changing the values of the filters' tuning parameters, hence the robustness of the method is testified. For this specific case characterized by smaller damage values, the outcomes of a parametric study is reported in Figure 12 to show once more the effects of a varying signal to noise ratio, so to assess the interplay between sensitivity to damage and measurement accuracy. Three levels of the RMS of the noise to signal ratio equal to 6%, 18% and 60% have been handled, which respectively correspond to standard deviations of the measurement error equal to 1, 3 and 10 mm. Figure 12 testifies that, while an increase in the noise level does not affect the ROM stiffness estimate (time histories can be hardly distinguished in the graph, as they are almost perfectly superposed to each other), it can drastically modify the convergence rate of subspace estimates.

Concerning the capability to track system evolution in case of incomplete measurements, namely if lateral displacements are not collected at all the storys, in Figure 13 an exemplary solution is reported for measurements not available at the 4$^{th}$ and 7$^{th}$ floors. While such incomplete measurements have again a marginal effect on the estimates of the ROM stiffness, they may lead to unidentifiability, or to a biased identification of the unobserved subspace components. Even though such outcome is rather expected from the system observability/ identifiability point of view, it must be stressed that the most important feature of the SHM approach, namely the capability to detect damage close to or in real time, is still preserved.

One final aspect to be discussed for the proposed coupled identification/tracking and model update technique, is linked to the computational gain attained. As partially reported in [20] the speedup, computed as the ratio between the time required to work on the full-order model (so, without any online update stage) and the time required to work instead on the ROM (including now the online update stage), is on the order of $1.5 - 2$, depending on whether the EKF-KF or the EK-PF-KF procedure is used. Although this value may depend on the features of the CPU running the procedure implemented in a (Matlab) code, the small reported values are due to the limited number of DOFs of the original full-order model of the structure, but still testify the positive trend toward SHM of shear type buildings close to real-time.

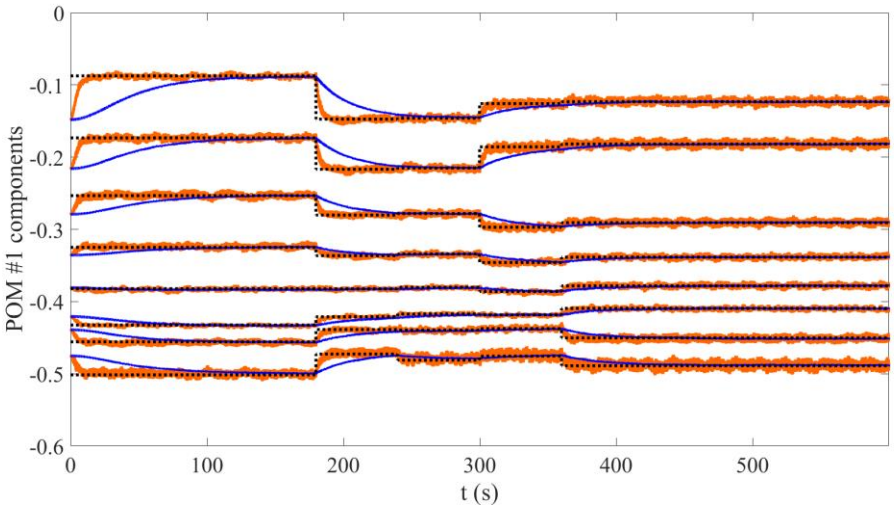


(a)

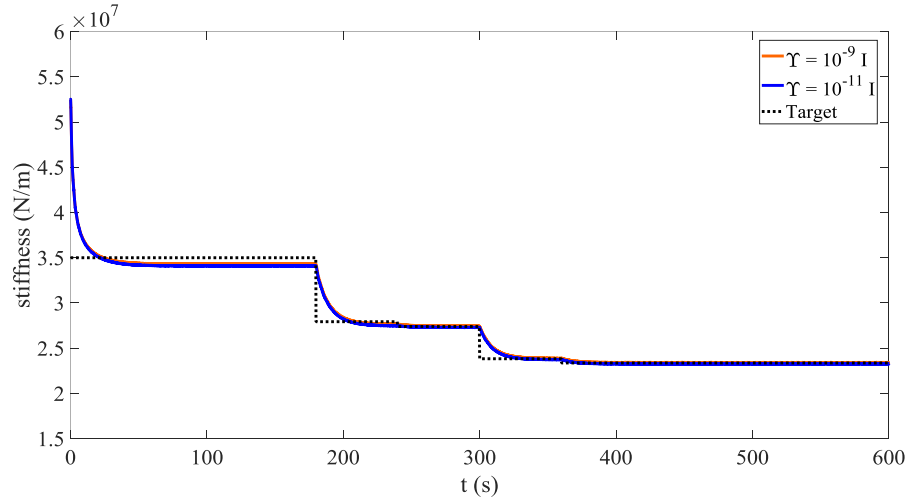


(b)

Figure 10: EK-PF-KF approach, 50% damage events: comparison between target (dashed lines) and estimated (continuous lines) time evolutions of (a) POM components and (b) MOR stiffness, at varying tuning noise covariance $\Upsilon$.

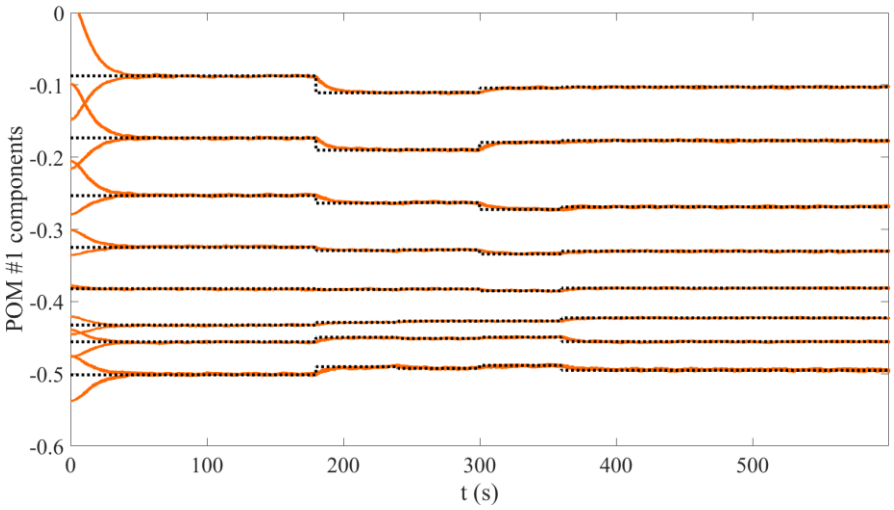


(a)

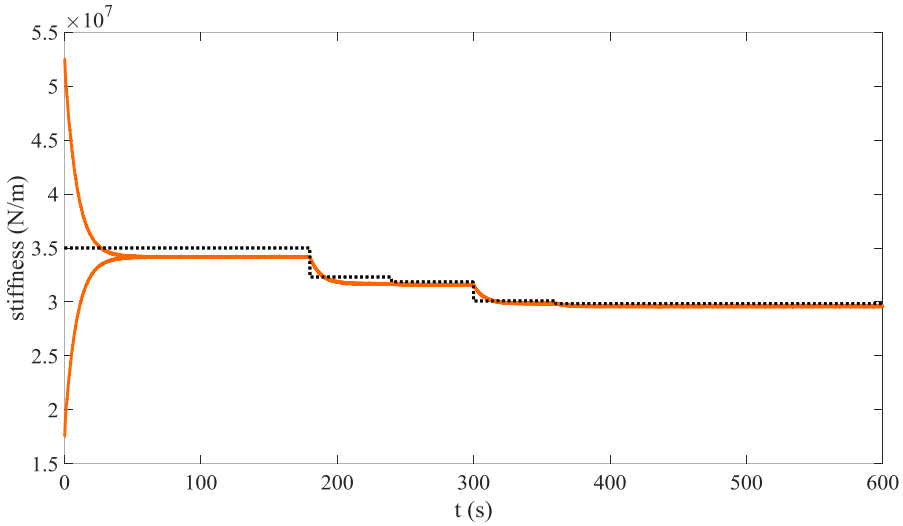


(b)

Figure 11: EK-PF-KF approach, 25% damage events: comparison between target (dashed lines) and estimated (continuous lines) time evolutions of (a) POM components and (b) MOR stiffness.

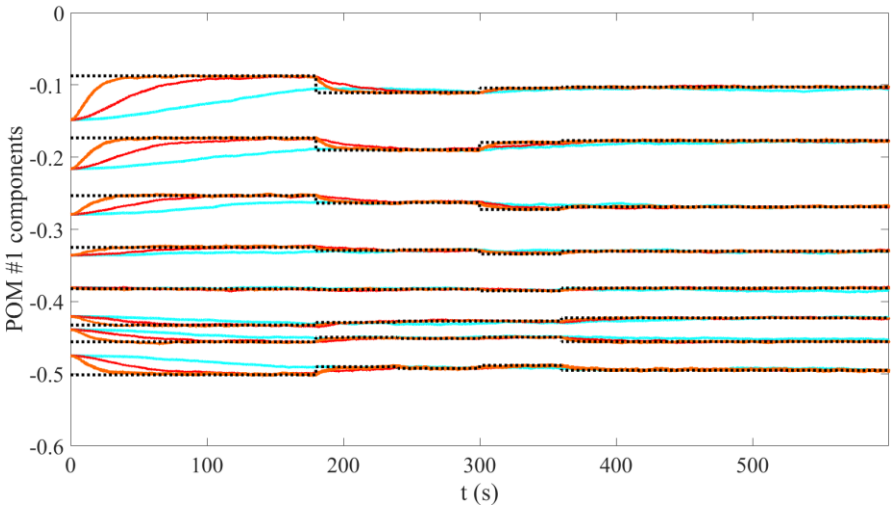


(a)

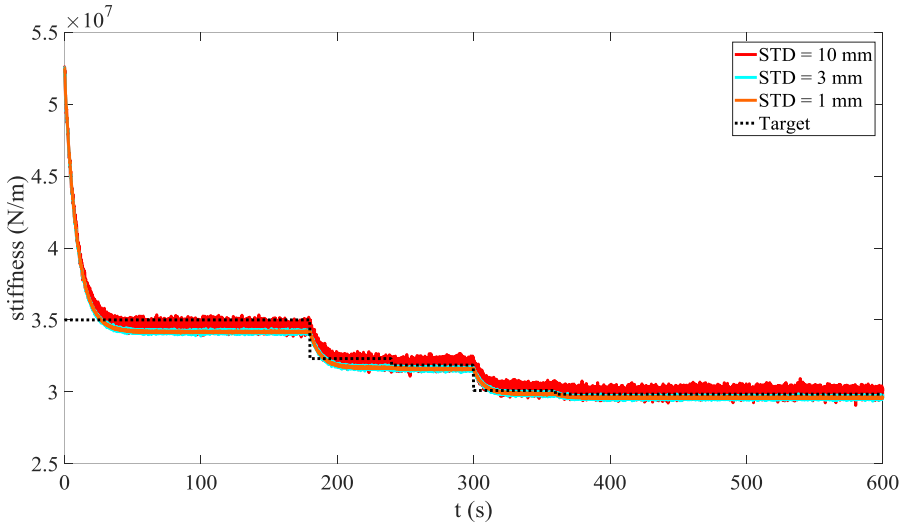


(b)

Figure 12: EK-PF-KF approach, 25% damage events: comparison between target (dashed lines) and estimated (continuous lines) time evolutions of (a) POM components and (b) MOR stiffness at varying noise level.

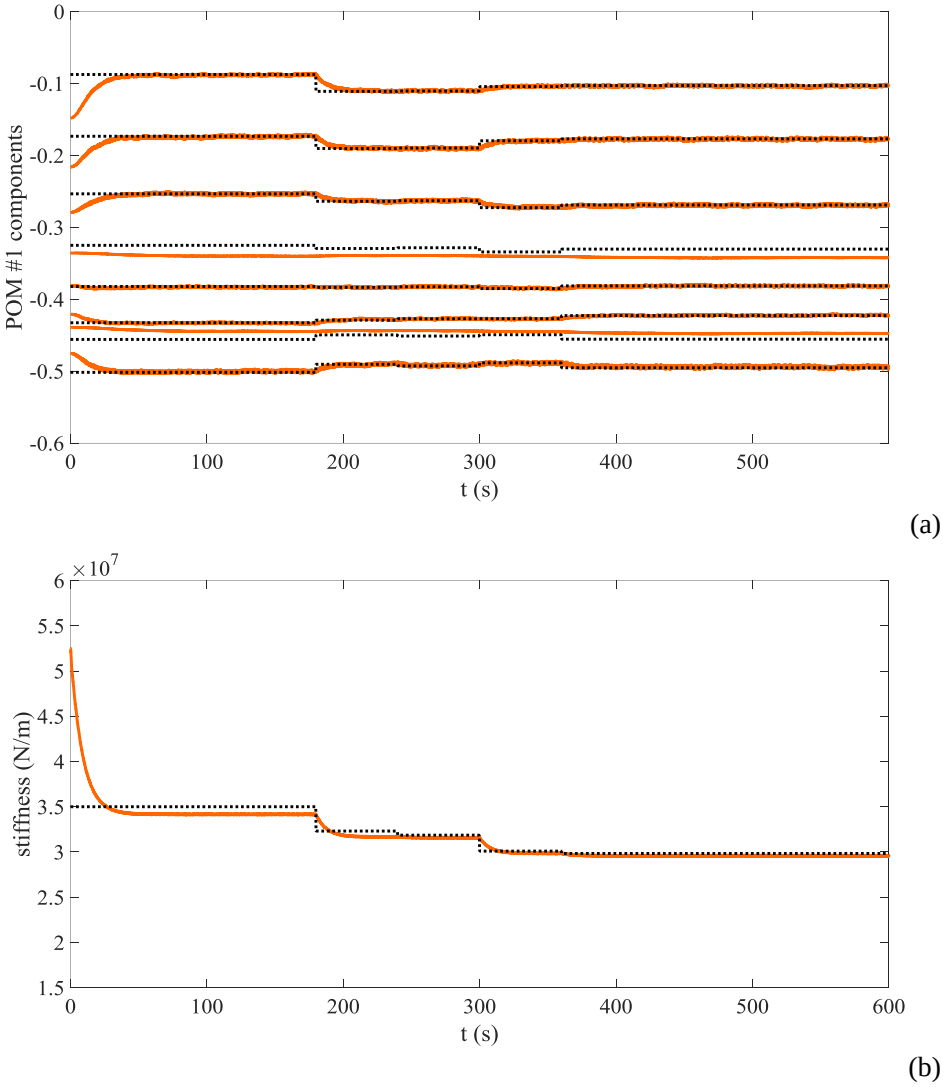


Figure 13: EK-PF-KF approach, 25% damage events: comparison between target (dashed lines) and estimated (continuous lines) time evolutions of (a) POM components and (b) MOR stiffness obtained with incomplete measurements (i.e. no measurements at 4$^{th}$ and 7$^{th}$ floors).

## 5. CONCLUDING REMARKS

In this paper, the joint estimation and reduced order modelling of a damaging structure has been investigated. As far as the reduced order modelling task is concerned, the proper orthogonal decomposition has been adopted to obtain a subset of the original full-order model DOFs that optimally represents the dynamics of the whole system. As far as the joint estimation

purpose is concerned, a hybrid extended Kalman particle filter has been proposed to track the ROM dynamics and identify the relevant stiffness properties online. In case of a time-varying damage state, instead of re-training the handled ROM a further Kalman filter has been adopted to exploit once more the available system observations and tune the components of the ROM mode(s) retained in the analysis.

Although the intricate procedure here proposed does not allow to easily set all the algorithmic parameters of the filtering procedures, it has been shown for a 8-story shear type building that the method can satisfactorily tune on-the-fly the ROM characteristics and also identify the varying stiffness properties of the structural ROM. Compared to an extended Kalman filter-based approach already proposed by the authors in [8] and to a standard particle filter-based one, the current methodology has shown interesting features in terms of stability of the estimates, and robustness against inaccuracies in the initialization values of the resulting Bayesian procedure.

In future works, the localization and quantification of the actual structural damage, which is spatially smeared or averaged by the ROM in the proposed procedure, will be further and better investigated. For this additional task, an artificial neural network (ANN) can be trained in the initial offline stage. In this regard, the reduced stiffness parameters and the components of the POMs can be used as input for the ANN. In a similar fashion, in [56] the variations of coefficients of an auto regressive model fitting the acceleration response of the structure, were adopted as damage sensitive features providing a means to successfuly identify the damage itself.

## REFERENCES

[1] J. Yang and S. Lin, "Identification of Parametric Variations of Structures Based on Least Squares Estimation and Adaptive Tracking Technique," *Journal of Engineering Mechanics*, vol. 131, pp. 290-298, 2005.

[2] P. Van Overschee and B. De Moor, *Subspace Identification for Linear Systems: Theory — Implementation — Applications*: Springer US, 1996.

[3] L. Chin-Hsiung, W. Jian-Huang, L. Yi-Cheng, L. Pei-Yang, and H. Shieh-Kung, "Structural damage diagnosis based on on-line recursive stochastic subspace identification," *Smart Materials and Structures,* vol. 20, p. 055004, 2011.

[4] B. Moaveni, X. He, J. Conte, J. Restrepo, and M. Panagiotou, "System Identification Study of a 7-Story Full-Scale Building Slice Tested on the UCSD-NEES Shake Table," *Journal of Structural Engineering,* vol. 137, pp. 705-717, 2010.

[5] B. Moaveni and I. Behmanesh, "Effects of changing ambient temperature on finite element model updating of the Dowling Hall Footbridge," *Engineering Structures,* vol. 43, pp. 58-68, 2012.

[6] S. Mariani and A. Corigliano, "Impact induced composite delamination: state and parameter identification via joint and dual extended Kalman filters," *Computer Methods in Applied Mechanics and Engineering,* vol. 194, pp. 5242-5272, 2005.

[7] E. N. Chatzi, A. W. Smyth, and S. F. Masri, "Experimental application of on-line parametric identification for nonlinear hysteretic systems with model uncertainty," *Structural Safety,* vol. 32, pp. 326-337, 2010.

[8] S. Mariani and A. Ghisi, "Unscented Kalman filtering for nonlinear structural dynamics," *Nonlinear Dynamics,* vol. 49, pp. 131-150, 2007.

[9] S. Eftekhar Azam, A. Ghisi, and S. Mariani, "Parallelized sigma-point Kalman filtering for structural dynamics," *Computers and Structures,* vol. 92-93, pp. 193-205, 2012.

[10] S. Eftekhar Azam and S. Mariani, "Dual estimation of partially observed nonlinear structural systems: A particle filter approach," *Mechanics Research Communications*, vol. 46, pp. 54-61, 2012.

[11] E. N. Chatzi and A. W. Smyth, "Particle filter scheme with mutation for the estimation of time-invariant parameters in structural health monitoring applications," *Structural Control and Health Monitoring*, vol. 20, pp. 1081-1095, 2013.

[12] D. Giagopoulos, A. Arailopoulos, S. E. Azam, C. Papadimitriou, E. Chatzi, and K. Grompanopoulos, "Dynamic response estimation and fatigue prediction in a linear substructure of a complex mechanical assembly," in *8th European Workshop on Structural Health Monitoring, EWSHM 2016*, 2016, pp. 890-899.

[13] S. Eftekhar Azam, *Online damage detection in structural systems*: Springer, 2014.

[14] E. N. Chatzi and A. W. Smyth, "Nonlinear System Identification: Particle based methods," in *Encyclopedia of Earthquake Engineering*, Beer M., Patelli E., Kougioumtzoglou I., and A. I., Eds., ed Berlin Heidelberg: Springer-Verlag, 2014, pp. 1-18.

[15] C. Papadimitriou and D.-C. Papadioti, "Component mode synthesis techniques for finite element model updating," *Computers & structures*, vol. 126, pp. 15-28, 2013.

[16] R. Ruotolo and C. Surace, "Using svd to detect damage in structures with different operational conditions," *Journal of Sound and Vibration*, vol. 226, pp. 425-439, 1999.

[17] S. Vanlanduit, E. Parloo, B. Cauberghe, P. Guillaume, and P. Verboven, "A robust singular value decomposition for damage detection under changing operating conditions and structural uncertainties," *Journal of Sound and Vibration*, vol. 284, pp. 1033-1050, 2005.

[18] U. Galvanetto and G. Violaris, "Numerical investigation of a new damage detection method based on proper orthogonal decomposition," *Mechanical Systems and Signal Processing*, vol. 21, pp. 1346-1361, 2007.

[19] C. Shane and R. Jha, "Proper orthogonal decomposition based algorithm for detecting damage location and severity in composite beams," *Mechanical Systems and Signal Processing*, vol. 25, pp. 1062-1072, 2011.

[20] S. Eftekhar Azam, S. Mariani, and N. K. A. Attari, "Online damage detection via a synergy of proper orthogonal decomposition and recursive Bayesian filters," *Nonlinear Dynamics*, pp. 1-23, 2017.

[21] S. S. Bisht and M. P. Singh, "An adaptive unscented Kalman filter for tracking sudden stiffness changes," *Mechanical Systems and Signal Processing*, vol. 49, pp. 181-195, 2014.

[22] R. A. De Callafon, B. Moaveni, J. P. Conte, X. He, and E. Udd, "General realization algorithm for modal identification of linear dynamic systems," *Journal of Engineering Mechanics*, vol. 134, pp. 712-722, 2008.

[23] K.-J. Bathe, *Finite element procedures*: Klaus-Jurgen Bathe, 2006.

[24] V. Buljak and G. Maier, "Proper orthogonal decomposition and radial basis functions in material characterization based on instrumented indentation," *Engineering Structures*, vol. 33, pp. 492-501, 2011.

[25] V. Dolci and R. Arina, "Proper orthogonal decomposition as surrogate model for aerodynamic optimization," *International Journal of Aerospace Engineering*, vol. 2016, 2016.

[26] H. Michael and V. Stefan, "Proper Orthogonal Decomposition Surrogate Models for Nonlinear Dynamical Systems: Error Estimates and Suboptimal Control," in *Dimension Reduction of Large-Scale Systems*. vol. Proceedings of a Workshop held in Oberwolfach, Germany, October 19–25, 2003, B. Peter, S. D. C., and M. Volker, Eds., ed Berlin Heidelberg: Springer 2005.

[27] G. Capellari, S. Eftekhar Azam, and S. Mariani, "Damage Detection in Flexible Plates through Reduced-Order Modeling and Hybrid Particle-Kalman Filtering," *Sensors*, vol. 16, p. 2, 2016.

[28] D. Xie, M. Xu, and E. H. Dowell, "Proper Orthogonal Decomposition Reduced-Order Model for Nonlinear Aeroelastic Oscillations," *AIAA Journal*, vol. 52, pp. 229-241, 2014.

[29] L. Sirovich, "Turbulence and the dynamics of coherent structures. I - Coherent structures. II - Symmetries and transformations. III - Dynamics and scaling," *Quarterly of Applied Mathematics*, vol. 45, pp. 573-590, 1987.

[30] S. Eftekhar Azam and S. Mariani, "Investigation of computational and accuracy issues in POD-based reduced order modeling of dynamic structural systems," *Engineering Structures*, vol. 54, pp. 150-167, 2013.

[31] A. Corigliano, M. Dossi, and S. Mariani, "Domain decomposition and model order reduction methods applied to the simulation of multiphysics problems in MEMS," *Computers and Structures*, vol. 122, pp. 113-127, 2013.

[32] A. Corigliano, M. Dossi, and S. Mariani, "Model order reduction and domain decomposition strategies for the solution of the dynamic elastic-plastic structural problem," *Computer Methods in Applied Mechanics and Engineering*, vol. 290, pp. 127-155, 2015.

[33] Y. C. Liang, H. P. Lee, S. P. Lim, W. Z. Lin, K. H. Lee, and C. G. Wu, "Proper Orthogonal Decomposition And Its Applications—Part I: Theory," *Journal of Sound and Vibration*, vol. 252, pp. 527-544, 2002.

[34] G. Kerschen and G. C. Golinval, "Physical interpretation of the proper orthogonal modes using the singular value decomposition," *Journal of Sound and Vibration* vol. 249, pp. 849-865, 2002.

[35] A. Corigliano and S. Mariani, "Parameter identification in explicit structural dynamics: performance of the extended Kalman filter," *Computer Methods in Applied Mechanics and Engineering*, vol. 193, pp. 3807-3830, 2004.

[36] C. Comi and S. Mariani, "Extended finite element simulation of quasi-brittle fracture in functionally graded materials," *Computer Methods in Applied Mechanics and Engineering*, vol. 196, pp. 4013-4026, 2007.

[37] A. Corigliano and S. Mariani, "Identification of a constitutive model for the simulation of time-dependent interlaminar debonding processes in composites," *Computer Methods in Applied Mechanics and Engineering*, vol. 191, pp. 1861-1894, 2002.

[38] L. Ljung, "Asymptotic behavior of the extended Kalman filter as a parameter estimator for linear systems," *Automatic Control, IEEE Transactions on*, vol. 24, pp. 36-50, 1979.

[39] K. Reif, S. Gunther, E. Yaz, and R. Unbehauen, "Stochastic stability of the discrete-time extended Kalman filter," *IEEE Transactions on Automatic Control*, vol. 44, pp. 714-728, 1999.

[40] S. J. Julier and J. K. Uhlmann, "A new extension of the Kalman filter to nonlinear systems," in *Int. symp. aerospace/defense sensing, simul. and controls*, 1997, p. 32.

[41] A. R. Ferreira da Silva, "Bayesian mixture models of variable dimension for image segmentation," *Computer Methods and Programs in Biomedicine*, vol. 94, pp. 1-14, 2009.

[42] A. Doucet and A. M. Johansen, "A tutorial on particle filtering and smoothing: Fifteen years later," *Handbook of Nonlinear Filtering*, 2009.

[43] F. Cadini, E. Zio, and D. Avram, "Monte Carlo-based filtering for fatigue crack growth estimation," *Probabilistic Engineering Mechanics*, vol. 24, pp. 367-373, 2009.

[44] N. J. Gordon, D. J. Salmond, and A. F. M. Smith, "Novel approach to nonlinear/non-Gaussian Bayesian state estimation," *Radar and Signal Processing, IEE Proceedings F*, vol. 140, pp. 107-113, 1993.

[45] M. S. Arulampalam, S. Maskell, N. Gordon, and T. Clapp, "A tutorial on particle filters for online nonlinear/non-Gaussian Bayesian tracking," *Signal Processing, IEEE Transactions on*, vol. 50, pp. 174-188, 2002.

[46] A. Doucet, "On sequential Monte Carlo methods for Bayesian filtering. ," *Statistics and Computing* vol. 10, pp. 197–208, 2000.

[47] J. D. Hol, T. B. Schon, and F. Gustafsson, "On Resampling Algorithms for Particle Filters," in *Nonlinear Statistical Signal Processing Workshop, 2006 IEEE*, 2006, pp. 79-82.

[48] G. Kitagawa, "Monte Carlo filter and smoother for non-Gaussian nonlinear state space models," *Journal of computational and graphical statistics*, vol. 5, pp. 1-25, 1996.

[49] P. Li, R. Goodall, and V. Kadirkamanathan, "Estimation of parameters in a linear state space model using a Rao-Blackwellised particle filter," in *IEE Proceedings: Control Theory and Applications*, 2004, pp. 727-738.

[50] S. Eftekhar Azam, E. Chatzi, C. Papadimitriou, and A. Smyth, "Experimental validation of the Kalman-type filters for online and real-time state and input estimation," *Journal of Vibration and Control*, vol. 23, pp. 2494-2519, 2017.

[51] C. Gentile and G. Bernardini, "An interferometric radar for non-contact measurement of deflections on civil engineering structures: laboratory and full-scale tests," *Structure and Infrastructure Engineering*, vol. 6, pp. 521-534, 2010.

[52] H. Jo, S. H. Sim, A. Tatkowski, B. Spencer, and M. E. Nelson, "Feasibility of displacement monitoring using low-cost GPS receivers," *Structural Control and Health Monitoring*, vol. 20, pp. 1240-1254, 2013.

[53] K.-V. Yuen, P. F. Liang, and S. C. Kuok, "Online estimation of noise parameters for Kalman filter," *Structural Engineering and Mechanics*, vol. 47, pp. 361-381, 2013.

[54] H. Mu and K.-V. Yuen, "Novel Outlier-Resistant Extended Kalman Filter for Robust Online Structural Identification," *Journal of Engineering Mechanics*, 2015.

[55] S. Eftekhar Azam, M. Bagherinia, and S. Mariani, "Stochastic system identification via particle and sigma-point Kalman filtering," *Scientia Iranica*, vol. 19, pp. 982-991, 2012.

[56] O. R. de Lautour and P. Omenzetter, "Damage classification and estimation in experimental structures using time series analysis and pattern recognition," *Mechanical Systems and Signal Processing*, vol. 24, pp. 1556-1569, 2010.

# APPENDIX A

Table A.1: the EKF-KF algorithm for time-varying damage states

- Initialization at time $t_0$:

$$\widehat{\boldsymbol{x}}_{r,0} = \mathbb{E}[\boldsymbol{x}_{r,0}] \quad \boldsymbol{P}_0 = \mathbb{E}\left[(\boldsymbol{x}_{r,0} - \widehat{\boldsymbol{x}}_{r,0})(\boldsymbol{x}_{r,0} - \widehat{\boldsymbol{x}}_{r,0})^{\mathrm{T}}\right]$$
$$\widehat{\boldsymbol{\varphi}}_{l,0} = \mathbb{E}[\boldsymbol{\varphi}_{l,0}] \quad \boldsymbol{P}_{ss,0} = \mathbb{E}\left[(\boldsymbol{\varphi}_{l,0} - \widehat{\boldsymbol{\varphi}}_{l,0})(\boldsymbol{\varphi}_{l,0} - \widehat{\boldsymbol{\varphi}}_{l,0})^{\mathrm{T}}\right]$$

- At time $t_k$, for $k = 1, \dots, N_t$:
  - Prediction stage:
    1. Evolve state and predict covariance:

$$\boldsymbol{x}_{r,k}^{-} = \boldsymbol{f}_{r,k}(\boldsymbol{x}_{r,k-1}, \boldsymbol{\mathcal{F}}_{l,k})$$
$$\boldsymbol{P}_k^{-} = \boldsymbol{F}_{r,k}\boldsymbol{P}_{k-1}\boldsymbol{F}_{r,k}^{T} + \boldsymbol{V}$$

    2. Evolve subspace and predict covariance:

$$\boldsymbol{\varphi}_{l,k}^{-} = \boldsymbol{\varphi}_{l,k-1}$$
$$\boldsymbol{P}_{ss,k}^{-} = \boldsymbol{P}_{ss,k-1} + \boldsymbol{\Upsilon}$$

  - Update stage:
    1. Use $\boldsymbol{\varphi}_{l,k}^{-}$ to estimate $\boldsymbol{L}_k$ and compute state Kalman gain:

$$\boldsymbol{G}_k = \boldsymbol{P}_k^{-}\boldsymbol{L}_k^{\mathrm{T}}\boldsymbol{H}^{\mathrm{T}}\left(\boldsymbol{H}\boldsymbol{L}_k\boldsymbol{P}_k^{-}\boldsymbol{L}_k^{\mathrm{T}}\boldsymbol{H}^{\mathrm{T}} + \boldsymbol{W}\right)^{-1}$$

    2. Update state and covariance:

$$\boldsymbol{x}_{r,k} = \boldsymbol{x}_{r,k}^{-} + \boldsymbol{G}_k(\boldsymbol{y}_k - \boldsymbol{H}\boldsymbol{L}_k\boldsymbol{x}_{r,k}^{-})$$
$$\boldsymbol{P}_k = \boldsymbol{P}_k^{-} - \boldsymbol{G}_k\boldsymbol{H}\boldsymbol{L}_k\boldsymbol{P}_k^{-}$$

    3. Compute subspace Kalman gain:

$$\boldsymbol{G}_{ss,k} = \boldsymbol{P}_{ss,k}^{-}\boldsymbol{H}_{ss}^{\mathrm{T}}\left(\boldsymbol{H}_{ss}\boldsymbol{P}_{ss,k}^{-}\boldsymbol{H}_{ss}^{\mathrm{T}} + \boldsymbol{W}\right)^{-1}$$

    4. Update subspace and covariance:

$$\boldsymbol{\varphi}_{l,k} = \boldsymbol{\varphi}_{l,k}^{-} + \boldsymbol{G}_{ss,k}(\boldsymbol{y}_k - \boldsymbol{H}_{ss}\boldsymbol{\varphi}_{l,k}^{-})$$
$$\boldsymbol{P}_{ss,k} = \boldsymbol{P}_{ss,k}^{-} - \boldsymbol{G}_{ss,k}\boldsymbol{H}_{ss}\boldsymbol{P}_{ss,k}^{-}$$

In this Appendix, we briefly discuss the EKF-KF approach that can be used in place of the EK-PF-KF one described in Section 3.2 for time-varying damage states, see [20].

The whole algorithm is detailed in Table A.1. Likewise the EK-PF-KF algorithm of Table 2, it consists in two filters running in parallel, one handling the update of the ROM state vector and the other one continuously tuning the POMs of the ROM itself. The former filter, which is centered on a linearization of the state transition providing on-the-fly the matrix $\boldsymbol{F}_{r,k}$, may still lead to the mentioned biases or divergent estimates already discussed in the text.